International Journal of Greenhouse Gas Control 67 (2017) 71–92

Contents lists available at ScienceDirect

International Journal of Greenhouse Gas Control

journal homepage: www.elsevier.com/locate/ijggc

Process integration study of tail-end Ca-Looping process for CO_2 capture in cement plants

E. De Lena[a], M. Spinelli[a], I. Martínez[a], M. Gatti[a], R. Scaccabarozzi[a], G. Cinti[b], M.C. Romano[a,*]

[a] Politecnico di Milano, Department of Energy, Via Lambruschini 4, 20156 Milano, Italy
[b] Italcementi, Via Camozzi 124, 24121 Bergamo, Italy

ARTICLE INFO

Keywords:
Cement
Ca-Looping
CO_2 capture
Post-combustion
Retrofitting

ABSTRACT

In this work, the integration of Calcium looping (CaL) process into a cement plant for post-combustion CO_2 capture is assessed via process simulations. In the proposed scheme, the carbonator of the CaL process is used as an end-of-pipe unit to capture the CO_2 from the cement kiln gas.

From the results obtained, it is demonstrated that CO_2 capture efficiencies of the order of 90% are achievable, with CaL reactors operating in conditions not far from those demonstrated for application in power plants. The integration of the tail-end CaL process results in a significant increase of the total fuel consumption (about two to three times higher) compared to the benchmark cement plant without CO_2 capture. On the other hand, the heat from the CaL process can be recovered by a steam cycle producing decarbonized electric power that may exceed the needs of the plant auxiliaries (including the ASU and the CO_2 compression and purification unit), exporting in this way electricity to the grid and so resulting in CO_2 emission credits from a life cycle perspective. The resulting specific primary energy consumption for CO_2 avoided (SPECCA) highly depends on the reference power generation technology considered, and it ranges between 2.7 and 3.7 MJ_{LHV}/kg_{CO2} in a coal-fired power generation scenario.

As for the retrofittability of existing cement plants, the operation of the suspension preheating tower after the implementation of the CaL unit, as well as the position of the CaL carbonator with respect to the raw mill, have been assessed. Based on the results obtained, no critical issues have been found from a technical point of view in the adoption of the tail-end CaL process in existing cement kilns.

1. Introduction

Cement production is an energy and carbon-intensive industry and one of the major industrial contributors to anthropogenic CO_2 emissions. World cement production has increased steadily over the years, amounting to around 4.1 Gt in 2015 (Olivier et al., 2016). CO_2 emissions from cement production come from fossil fuel combustion and limestone calcination. About 60% of the CO_2 emissions in a cement plant comes from the calcination of the limestone that is used as raw material, whereas the remaining 40% comes from the combustion of fossil fuels that supply the heat needed for clinker production and for limestone calcination. In 2015, CO_2 emissions from cement production accounted for about 8% of the global anthropogenic CO_2 emissions (Olivier et al., 2016). Among the different methods proposed for reducing CO_2 emissions in the cement industry there are the use of fossil fuels with low carbon content (e.g. natural gas), the use of carbon neutral fuels (e.g. biomass), the thermal efficiency improvement, the reduction of the clinker/cement ratio by using a larger fraction of additives in the final cement (IEA, 2009). However, the CO_2 emission reduction potential of these measures is limited because they do not tackle the emissions derived from limestone calcination. Therefore, to achieve significant cuts in CO_2 emissions in a cement production process, it is necessary to implement Carbon Capture and Storage (CCS) techniques (IEAGHG, 2013).

Different CO_2 capture technologies have been investigated to be integrated in a cement production process, including oxy-combustion, post-combustion absorption, membranes and Ca-Looping (Hills et al., 2016; IEAGHG, 2013, 2008; Scholes et al., 2014; Vatopoulos and Tzimas, 2012). This work focuses on the process integration of the Ca-Looping (CaL) process into a cement plant. This capture technology is

* Corresponding author.
E-mail address: matteo.romano@polimi.it (M.C. Romano).

http://dx.doi.org/10.1016/j.ijggc.2017.10.005
Received 25 June 2017; Received in revised form 14 October 2017; Accepted 15 October 2017

Nomenclature

E_{carb}	Carbonator efficiency [%]
e_{CO2}	Specific CO_2 emissions [kg_{CO2}/t_{clk}]
E_{eq}	Carbonator efficiency at equilibrium conditions [%]
F_0	Limestone make-up flow rate [kmol/s]
F_{Ca}	Calcium flow rate circulating between reactors in the Ca-Looping system [kmol/s]
F_{CO2}	CO_2 flow rate fed to the carbonator of the Ca-Looping system [kmol/s]
k	Deactivation constant for the CaO decay activity law in Eq. (2) [-]
N	Number of calcination-carbonation cycles undergone by a CaO particle
P_e	Net plant absorbed power [MW_e]
q	Specific fuel consumption [MJ_{LHV}/t_{clk}]
r_N	Fraction of CaO particles having circulated N times through the calcination-carbonation loop [-]
X_{ave}	Average maximum conversion of CaO in the Ca-Looping system [%]
X_r	Residual activity of CaO particles having undergone a high number of calcination-carbonation cycles [%]
Ws	Solid inventory in the carbonator [kg/m^2]

Subscripts

carb	Carbonator
cem	Cement
clk	Clinker
e	Electric
eq	Equivalent
ref	Reference plant (without CO_2 capture)

Greek letters

η	Efficiency

Acronyms

ASU	Air separation unit
CaL	Calcium-looping
CCS	Carbon capture and storage
CFB	Circulating fluidized bed
CPU	CO_2 purification unit
FWH	Feed water heater
HRSC	Heat recovery steam cycle
IL	Integration level
LCA	Life cycle assessment
LHV	Lower heating value
ORC	Organic Rankine cycle
PC	Pulverized coal
SPECCA	Specific primary energy for CO_2 avoided [MJ_{LHV}/kg_{CO2}]
TSA	Temperature swing adsorption
USC	Ultra-supercritical

one of the most promising ones for CO_2 capture in cement plants (Abanades et al., 2015; Bosoaga et al., 2009; Dean et al., 2011a; Spinelli et al., 2017). It was orginally proposed by Shimizu et al. (1999) and it is based on the reversible reaction between CaO and CO_2 at high temperature. Flue gas containing CO_2 is put into contact with a solid stream containing CaO in a carbonator reactor operating at about 650 °C, where the exothermic carbonation reaction occurs (1). Solids containing the $CaCO_3$ formed by the carbonation reaction are sent to a separate reactor or calciner for regeneration at a temperature of 900–950 °C. The high temperature needed in this reactor for the endothermic calcination of $CaCO_3$ under high CO_2 partial pressures is achieved by burning additional fuel in the reactor with oxygen. This CaL process has been successfully demonstrated up to 1–2 MW_{th} scale (Arias et al., 2013; Ströhle et al., 2014) in operating conditions representative of the integration in coal-fired power plants, where flue gas has lower CO_2 concentration compared to cement kilns.

$$CaO + CO_2 \leftrightharpoons CaCO_3 \quad \Delta H_{298K} = -178.8 kJ/mol \tag{1}$$

One of the inherent advantages of this technology is that most of the fuel chemical energy introduced into the calciner can be recovered as high temperature heat in the process and potentially converted into electricity with high efficiency. Moreover, the CaO-based sorbent derives from natural sources (i.e. limestone), which is characterised by low cost and wide availability. One drawback of the process is the need of a continuous make-up of fresh limestone to compensate the purge of solids from the CaL loop, which is needed to: (i) avoid build-up of coal ash and $CaSO_4$ originating from coal combustion in the calciner and (ii) keep a proper activity of the sorbent, which reduces with the number of carbonation-calcination cycles. On this regard, the integration of the CaL process in a cement plant provides synergies because the amount of limestone needed for clinker production largely exceeds the make-up need of the CaL process and the CaO-rich purge can be conveniently used in the cement kiln for clinker production. In this way, the drawbacks of needing a relatively large limestone make-up and of managing the solid purge disappear. For the same reason, cement plants are often proposed as sinks for the spent CaO from CaL units integrated in power plants, where the CaL purge can be valorized by producing clinker with lower CO_2 emissions and lower fuel consumption with no changes in the cement kiln equipment (Martínez et al., 2016). Some recent works have confirmed that cement clinker can be produced using the CaL system purge (Dean et al., 2011b; Telesca et al., 2015), which is mainly composed of CaO and minor fraction of $CaSO_4$ and ash, improving the burnability index of the raw material with respect to a conventional raw meal (Telesca et al., 2014).

Different possibilities for integrating a CaL system into a cement plant have been proposed in the literature, which differ in the level of integration between the CaL process and the clinker production process. The most straightforward process integration option is the tail-end configuration (Fig. 1(a)), where the CaL process is integrated as an end-of-pipe process, treating the cement kiln exhaust gas in the carbonator (Atsonios et al., 2015; Martínez Vera, 2009; Ozcan et al., 2013; Spinelli et al., 2017; Trevino and Martínez, 2009; Vatopoulos and Tzimas, 2012). In this case, a fraction of the limestone fed to the cement kiln is introduced in the calciner of the CaL process to be used as a CO_2 sorbent. The CaO-rich solid purge from the CaL process is then introduced into the clinker burning line for replacing part of the limestone in the raw meal. In this configuration, the cement kiln is assumed to be a conventional one, hence including the rotary kiln, pre-calciner, suspension preheater and clinker cooler. The operation of the CaL process in conditions representative for this process integration option has been recently demonstrated in two different facilities, at 30 kW_{th} and 200 kW_{th} scale (Arias et al., 2017; Hornberger et al., 2017).

Alternatively, a highly integrated configuration between the CaL process and the clinker burning line is also possible, as depicted in Fig. 1(b). In this case, the carbonator is integrated into the pre-heating tower and only one oxyfuel calciner is used, operating as both raw meal pre-calciner and as CaL process calciner (Marchi et al., 2012a,b; Rodríguez et al., 2012; Romano et al., 2014; Spinelli et al., 2017). Raw meal is preferably used as sorbent in this case, so that separate pre-heating and calcination lines for high purity limestone and other raw meal correctives (which may contain limestone as well, depending on the properties of the raw material from the quarry) are avoided. The intrinsic advantage of the integrated CaL configuration is that a single oxyfuel calcination is performed, which implies a noticeable saving in the fuel consumption of the plant (Spinelli et al., 2017). On the contrary, in the tail-end configuration, a double calcination reaction is needed to capture the CO_2 originated from the limestone fed to the plant. A first calcination occurs in the air-blown pre-calciner, where the CO_2 contained in the raw meal is released. Afterwards, this CO_2 is separated from flue gases in the carbonator of the CaL process by forming $CaCO_3$, which is calcined again in the oxyfired calciner of the CaL unit.

An important issue to be considered when defining the process integration in the cement plant is the particle size. Cement kiln must be fed with sufficiently fine material to ensure proper formation of the clinker phases along the rotary kiln. Average size of raw meal particles (d_{50}) is 10–20 μm, which corresponds to Geldart particle group C (cohesive particles). Due to the difficulty in fluidizing this kind of material, entrained flow reactors should be preferred over fluidized bed when the CaL system uses the same material as in the rotary kiln, such as in the integrated configuration shown in Fig. 1(b). When using the purge from a fluidized bed CaL system for clinker production, it should be taken into account that this kind of reactor typically operates with larger particle sizes of 100–300 μm from Geldart's particle group B. Therefore, in this case, the solid purge needs to pass through the raw mill with the other raw material constituents to be properly mixed and ground to a suitable particle size for clinker production.

In this paper, a process integration study and simulation of a tail-end CaL configuration into a cement kiln is presented. This work presents the most comprehensive study today available in the literature on this topic. Compared to previous studies on this CaL process integration concept, the paper collects the following novelties: (i) it presents a wider sensitivity analysis on CaL process parameters; (ii) it discusses in detail the configuration of the heat recovery steam cycle, which is based on a cycle configuration and steam parameters suitable for its power output; (iii) it considers the constrain set by the clinker production process on the size of the raw meal particles to be fed to the rotary kiln; (iv) it compares novel configurations, assessing the effect of using the CaL unit for recovering the CO_2 in the vent gas of the CO_2 purification unit and the position of the carbonator (before or after the raw mill); (v) it discusses a retrofittability study for the application of this process in an existing cement kiln; (vi) it includes the effect of indirect fuel consumptions and indirect CO_2 emissions associated to the electric balance

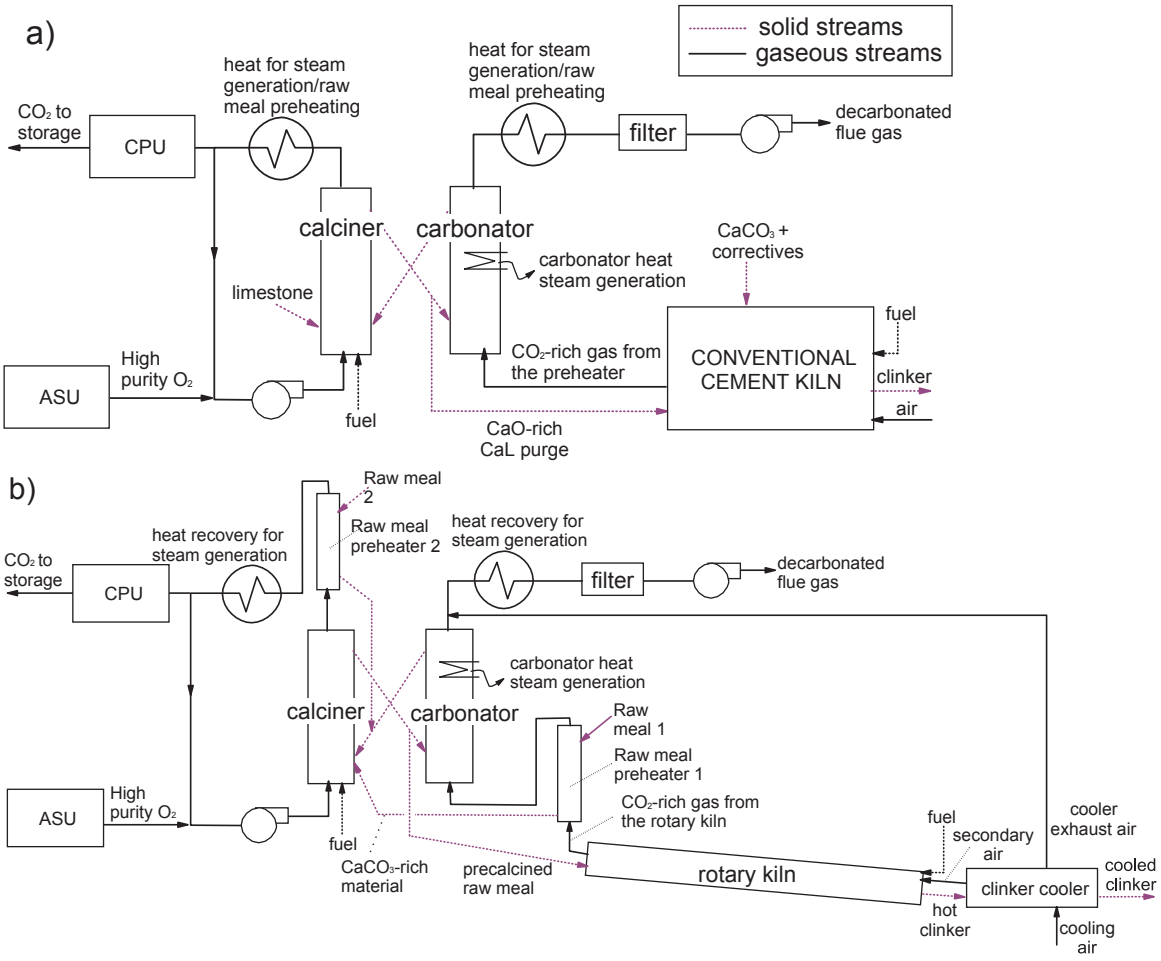

Fig. 1. Conceptual scheme for the integration of a CaL process into a cement plant: (a) tail-end configuration; (b) highly integrated configuration using raw meal as CO_2 sorbent precursor.

of the cement plant, comparing several power generation technology scenarios. Process simulations are based on a carbonator reactor model, a full cement kiln process model and a heat recovery steam cycle model, as discussed in Section 2. After presenting the key performance indicators (Section 3), a wide sensitivity analysis is performed on the main CaL process parameters (Section 4) and the retrofittability of the process in existing cement kilns is discussed (Section 4.1). The effects of the efficiency of the heat recovery steam cycle (Section 4.2) and of different heat integration options (Section 4.3) on the key performance parameters are finally described.

2. Process description and assumptions

2.1. Clinker burning process

The clinker production process is designed on the Best Available Technique (BAT) standard as defined in the European BREF document for the manufacture of cement (Schorcht et al., 2013). This process constitutes the core of the reference cement plant without CO_2 capture, and it remains practically unchanged when integrated with the CaL process. In Fig. 2, the cement kiln with CaL process for CO_2 capture is shown, indicating the components of the conventional kiln and the components of the CaL CO_2 capture island. The clinker burning process, which is based on a dry kiln process, consists of a five-stage cyclone preheater, a pre-calciner with a tertiary air duct, a rotary kiln and a grate clinker cooler. The cement kiln considered in this work has a clinker capacity of around 3000 t/d (raw meal/clinker factor of 1.6), which is a representative size for a European cement plant. This size corresponds to a yearly clinker production of 1 Mt (accounting for a run time of more than 330 d/yr) and a cement production of 1.36 Mt/yr. Main process assumptions used for carrying out the simulation of the cement burning line are summarized in Table 1. Assumptions related to the clinker burning line (e.g. fuel consumptions, calcination degree, cyclones efficiency, false air in-leakages) have been defined according to the model developed by the German Cement Works Association VDZ for the European Cement Research Academy (ECRA) (Hoenig et al., 2012) and the IEA Greenhouse Gas R & D Programme (IEAGHG, 2013). The model developed for the reference cement kiln has been successfully validated against the original VDZ model. More details on the process model and the validation process are available in public CEMCAP deliverable (CEMCAP, 2016).

Raw meal used for clinker production consists mainly of $CaCO_3$, coming from limestone or marl, and oxides of Si, Fe and Al, which are typically introduced through additional raw materials in order to achieve the targeted composition. The raw meal is ground in the raw mill, where it is also dried via direct contact with hot gas coming from the preheating tower. The dried raw meal from the raw mill, whose composition is given in Table 2, is heated up in a five-stage suspension (or cyclone) preheater. The raw material is fed to the top of the preheating tower and it is preheated sequentially from the first to the fifth stage (counted starting from the top of the tower) against the hot exhaust gas flowing from the bottom to the top (i.e. from the fifth to the first cyclone). Each suspension preheater stage is composed of a duct, where solid particles are entrained upwards and heated up by the gas, and a cyclone which separates the solids and distributes them to the following stage towards the bottom of the tower. As indicated in Table 1, solid separation efficiency, heat losses and air in-leakages in each suspension preheater stage are considered in the simulation. As

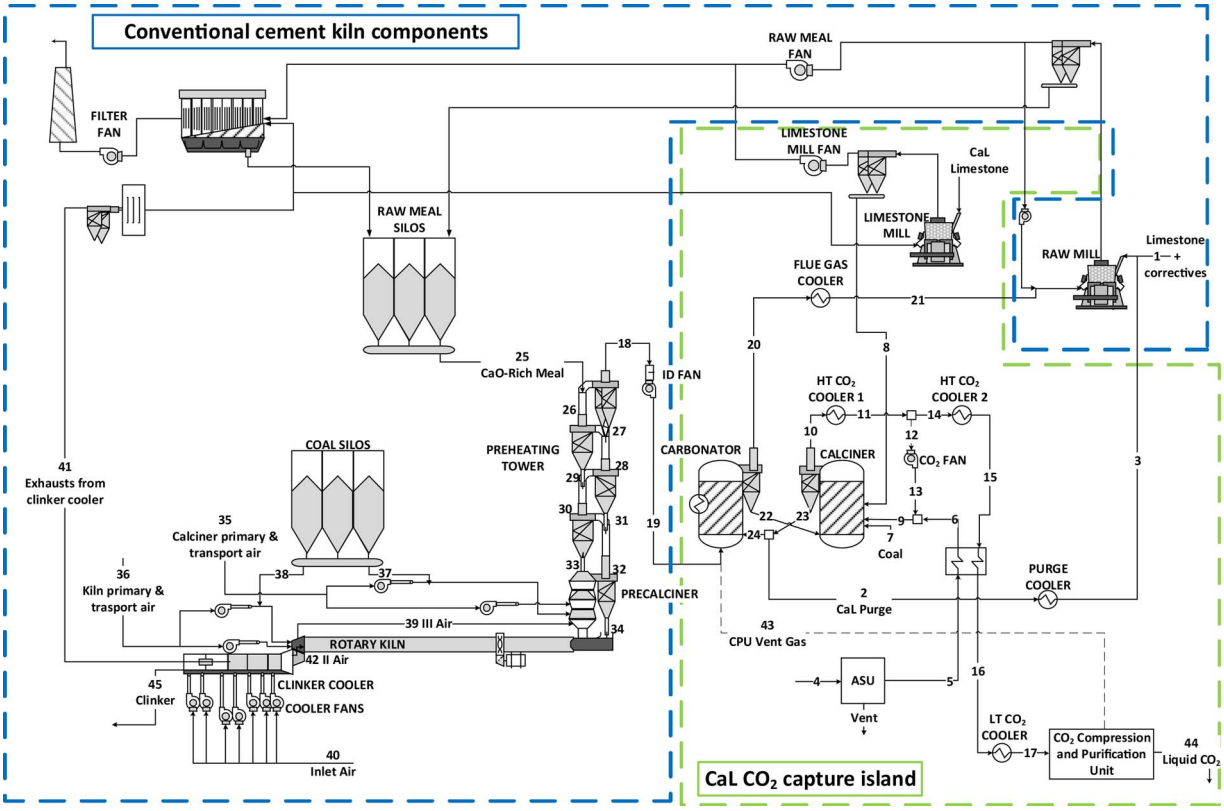

Fig. 2. Process configuration of the cement kiln with CO_2 capture by tail-end CaL process. Properties of the streams of the base case CaL cement kiln with Integration level (IL) = 20%, carbonator solid inventory (Ws) = 1000 kg/m^2 and carbonator efficiency (E_{carb}) = 90% are reported in Table A1 in the Appendix A.

Table 1
Main assumptions used for the simulations.

Clinker burning line	
Clinker production [tpd]	2825
Clinker/cement factor	0.737
Electric consumption of auxiliaries [kWh_e/t_{cem}]	97
Cyclones efficiency (1st / 2nd / 3rd / 4th stage) [%]	96 / 86 / 86 / 86
Pre-calciner cyclone efficiency [%]	75.6
Primary and transport air to pre-calciner [$Nm^3/kg_{coal\ to\ pre\text{-}calciner}$]	0.24
Primary and transport air to rotary kiln [$Nm^3/ kg_{coal\ to\ rotary\ kiln}$]	1.74
Secondary air to rotary kiln [Nm^3/t_{clk}]	259.7
Tertiary air to pre-calciner [Nm^3/t_{clk}]	622.4
Coal input to rotary kiln [kJ_{LHV}/kg_{clk}]	1210
Pre-calciner outlet temperature [°C]	861.8
Rotary kiln gas outlet temperature [°C]	1078.5
Secondary air temperature [°C]	1137.0
Tertiary air temperature [°C]	1049.8
Clinker temperature at cooler outlet [°C]	114.9
Temperature of solids after milling and crushing [°C]	60.0
Ambient temperature [°C]	15.0
Calcination degree at pre-calciner outlet[%]	94.2
Heat losses from rotary kiln [kJ_{th}/kg_{clk}]	180.2
Heat losses from pre-calciner [kJ_{th}/kg_{clk}]	95.64
Heat losses from clinker cooler [kJ_{th}/kg_{clk}]	11.13
Heat losses from preheating tower [kJ_{th}/kg_{clk}]	19.02
Air in-leakages into rotary kiln [Nm^3/t_{clk}]	11.98
Air in-leakages into pre-calciner [Nm^3/t_{clk}]	6.4
Air in-leakages into pre-calciner cyclone [Nm^3/t_{clk}]	6.4
Air in-leakages into preheating tower (1st / 2nd / 3rd / 4th stage) [Nm^3/t_{clk}]	18.8 / 9.4 / 9.4 / 9.4
Ca-Looping process	
Fans isentropic efficiency [%]	82
Fans electric-mechanical efficiency [%]	94
Carbonator outlet temperature [°C]	650
Carbonator solid inventory [kg/m^2]	1000
Pressure losses in carbonator, cyclones, back pass and filters [kPa]	20
Gas superficial velocity at carbonator inlet [m/s]	5
Calciner outlet temperature [°C]	920
Pressure losses in calciner [kPa]	15
Recycle gas temperature [°C]	400
Oxygen concentration in oxidant flow to calciner [%vol.]	50
Oxygen preheating temperature [°C]	150
Oxygen concentration in calciner off-gas [%vol.]	5
Auxiliaries for calciner fuel grinding [kWh_e/kg_{coal}]	0.0083
Air separation unit	
Oxygen purity [%vol.]	95
Electric consumption [kWh/t_{O2}]	226
LP steam consumption for TSA regeneration [kJ/kg_{O2}]	58.3
Heat recovery steam cycle	
Evaporation pressure [bar]	100
Superheated steam temperature [°C]	530
Condensing pressure [bar]	0.07
Steam turbine isentropic efficiency [%]	85.7
Steam turbine mechanical-electric efficiency [%]	97
Feedwater pump hydraulic efficiency [%]	75
Feedwater pump mechanical-electric efficiency [%]	94
Electric consumption for heat rejection to ambient [% of the heat rejected]	1
Pressure drop in the economizer [bar]	20
Pressure drop in superheater [%]	8
Pressure drop in turbine admission valve [%]	5
LP steam bleeding pressure [bar]	0.35
Deaerator temperature [°C]	140
Pressure drop of the bled steam to deaerator [%]	7
Pressure drop of the bled steam to surface preheater [%]	5
Pinch point temperature difference in the surface FWH [°C]	3
Water-condensate temperature difference in surface FWH [°C]	5
Pinch point temperature difference in steam generator [°C]	10
CO_2 *compression and purification unit*	
Pressure in the CO_2 purification vessel [bar]	17.3
Temperature in the CO_2 purification vessel [°C]	−54
Number of LP/HP intercooled compression stages	3 / 2
Minimum ΔT in the main heat exchanger [°C]	2
IC compressor isentropic efficiency LP/HP [%]	82 / 84
IC compressor mechanical efficiency LP/HP [%]	94 / 92
Last stage IC compressor CO_2 discharge pressure [bar]	89.1
Pump mechanical efficiency [%]	90
Pump hydraulic efficiency [%]	75
CO_2 purity [%vol.]	> 95%
CO_2 delivery pressure [bar]	150
CO_2 delivery temperature [°C]	35
Equivalent electric consumption for dehydration [kWh_e/t_{CO2}]	3

depicted in Fig. 2, additional cyclones and dust filters are needed downstream of the raw mill to separate the entrained solids before sending the exhaust gas to the stack. Electric consumptions of the fans included in the exhaust gas line ('Raw meal fan' and 'Filter fan' shown in Fig. 2) are included in the overall specific electric consumption of the clinker production process given in Table 1.

As highlighted in Fig. 2, the preheated solids at the exit of the fourth suspension preheater stage (stream #33) are fed to the pre-calciner, where most of the $CaCO_3$ contained in the raw meal is calcined into CaO and CO_2. Energy needed for this endothermic reaction is provided by the combustion of coal (Table 3), using low temperature primary transport air (#35) and high temperature tertiary air from the clinker cooler at 1050 °C (#39). Flue gas leaving the rotary kiln at 1078 °C also flows through the pre-calciner. Calcination degree (defined as the ratio between the moles of CaO and the total moles of Ca at calciner exit) of around 94% is reached in the pre-calciner, which operates with an outlet temperature of 862 °C. Pre-calcined raw meal and calciner off-gas enter the last cyclone of the preheating tower where solids are separated and fed to the rotary kiln (#34), whereas flue gas (#32) flows upwards and enters the duct of the fourth cyclone, located above.

The rotary kiln represents the core of the clinker production process. In this reactor, the completion of the $CaCO_3$ calcination and the formation of the main clinker constituents occur. The kiln is a long refractory lined tube, slightly inclined towards the clinker discharge end, that rotates at 1.3–3.5 revolutions per minute. As a result of the combination of kiln rotation and inclination, the solid-liquid material moves towards the hot end of the reactor, where coal combustion occurs. The combustion air in the rotary kiln comes from the clinker cooler ('secondary air', #42, about 90%), from the primary air and from the transport air (#36) that is directly fed to the kiln burner with the coal (#38). After the combustion zone, the flue gas moves towards the pre-calciner, in counter-current with the solids. As the solid phase moves towards the rotary kiln burner, the different clinker phases are formed thanks to the high temperature. Temperature of about 1450 °C is reached by the hot clinker at the end of the kiln, before being discharged to a grate cooler.

In the clinker cooler, clinker is rapidly cooled down to minimize the formation of undesired coarse crystals that would lead to erratic cement setting, at the same time preventing the dissociation of alite ($3CaO{\cdot}SiO_2$), the most important clinker constituents which provides the required properties to clinker, in belite ($2CaO{\cdot}SiO_2$) and free lime (CaO). Clinker is transported over a reciprocating grate, through which the cooling air flows in cross flow arrangement. Ambient air (#40) is used as cooling medium in the clinker cooler. Most of this air is heated up to a very high temperature and then used as secondary and tertiary combustion air in the rotary kiln and the pre-calciner, respectively. An almost equivalent stream of air at lower temperature (~300 °C) is generated in the final part of the clinker cooler (#41), which is ultimately emitted to the atmosphere after filtration.

The main constituents of clinker are Alite ($3CaO{\cdot}SiO_2$ or C3S), Belite ($2CaO{\cdot}SiO_2$ or C2S), Calcium Aluminate ($3CaO{\cdot}Al_2O_3$ or C3A) and Ferrite ($4CaO{\cdot}Fe_2O_3{\cdot}Al_2O_3$ or C4AF), with a typical final composition of

Table 2
Raw meal composition (wt.%), after drying.

$CaCO_3$	79.08
SiO_2	13.77
Al_2O_3	3.33
Fe_2O_3	2.01
$MgCO_3$	1.53
Moisture	0.28

Table 3
Coal composition and heating value.

Coal composition, wt.%	
C	69.00
H	4.00
S	0.50
N	0.48
O	9.00
Ash	16.50
Moisture	0.50
Lower Heating Value, MJ/kg	27.0
Ash composition, wt.%	
SiO_2	43.70
Al_2O_3	32.42
CaO	18.18
Fe_2O_3	4.00
MgO	1.70

65%wt. of C3S, 15%wt. of C2S, 10%wt. of C3A and 10%wt. of C4AF (Suhr et al., 2015). Smaller amounts of other components like MgO, CaO, K_2SO_4, Na_2SO_4 and $CaSO_4$ also appear in the final clinker. Clinker exiting the cooler is ultimately ground and mixed with gypsum (bi-hydrate calcium sulphates) and/or other materials like pozzolana, limestone, fly ash and slag to make cement.

2.2. Ca-Looping system

A system of two interconnected circulating fluidized bed (CFB) reactors is considered for the carbonator and the calciner of the CaL system.

In the baseline configuration, the carbonator of the CaL system is placed between the preheating tower and the raw mill as depicted in Fig. 2. Exhaust gas exiting the preheater tower at about 330 °C (stream #18) is compressed by the cement kiln induced draft (ID) fan to be introduced into the carbonator reactor. The CO_2-depleted gas from the carbonator (#20) has a reduced flow rate due to the removal of most of the CO_2, but it exits the carbonator at 650 °C, with a sensible heat content which exceeds the heat requirement for raw meal drying. Therefore, the decarbonized flue gas stream is cooled to a temperature of about 430 °C (#21) before mixing with a recycle stream for temperature moderation and entering the raw mill. For the ease of retrofit of an existing cement plant, the most preferable configuration is to place the carbonator of the CaL system downstream the raw mill (i.e. stream #19 in Fig. 2 enters first the raw mill and then the carbonator), avoiding in this way any change of the raw mill operation. The drawback of this configuration is related to the high air infiltration in the mill, causing a significant increase of the flow rate and a reduction of the CO_2 concentration of the flue gas to be treated in the carbonator, with a consequent increase of carbonator size and cost. This alternative configuration is discussed further on in Section 4.1.

The carbonator reactor is operated at the typical temperature of 650 °C (Martínez et al., 2016) and the solids exiting this reactor (#22) are sent to the calciner, where oxy-combustion of coal is carried out to calcine the $CaCO_3$ formed in the carbonator. Complete calcination (i.e. 100% calcination degree) and a calciner outlet temperature of 920 °C are assumed in the oxyfired calciner. Higher calcination temperature than in the pre-calciner of the cement kiln is needed to allow calcination under the higher CO_2 partial pressure conditions in this reactor. The selected calcination temperature is 35–40 °C above the calcination equilibrium temperature in the obtained CO_2-rich atmosphere, which is a sufficient margin to justify the assumed complete calcination (Martínez et al., 2013). The same coal used in the clinker production process is considered to be burned in the CaL calciner. A cryogenic Air Separation Unit (ASU) produces 95% pure oxygen to be used as oxidant in the CaL calciner. Electric consumption of the ASU has been defined taking into account the size of plant and have been assumed equal to 226 kWh/t_{O2} (Queneau and Marcuson, 1996). Low pressure steam is condensed in the ASU to provide a heat of 58.3 kJ/kg_{O2} for the regeneration of the TSA bed for front end air purification (IEAGHG, 2005). A CO_2 recycle (#13) acts as temperature moderator, by reducing O_2 concentration in the oxidant stream at calciner inlet down to 50% on a molar basis.

The rich-CO_2 stream generated in the calciner of the CaL process achieves a CO_2 purity of around 90% (on a dry molar basis), due to the oxidant excess required for ensuring complete combustion and to the residual N_2 and Ar impurities contained in the oxygen stream from the ASU. Since the purity required for the final storage of CO_2 may range from 95 to 99%mol depending on the storage site (Pipitone and Bolland, 2009), a CO_2 purification unit (CPU) is needed. The CPU considered in this work is based on a conventional single stage phase-change based separation auto-refrigerated scheme (Shah, 2011). The CO_2-rich stream to be purified is compressed up to a pressure of 19.6 bar in a three-stage intercooled compressor, dehydrated and cooled down to −45 °C in a counter-current heat exchanger featuring both the non-condensable gas stream at −54 °C and the purified CO_2 as cold sinks. CO_2 dehydration was assumed to consume LP steam and electricity, causing an equivalent electric power consumption of 3 $kW_e/(t_{CO2}/h)$ (IEAGHG, 2014). Pressure after the first three intercooled stage compression section, which determines the pressure of the knock-out drum, has been selected in order to obtain a purified liquid CO_2 stream with purity higher than 95%. The partial liquefaction of the CO_2-rich stream to be purified is achieved thanks to the refrigeration effect provided by the purified liquid CO_2 stream. Indeed, the purified liquid CO_2 stream, after separation in the knock-out drum, is flashed to 13.5 bar and −55.7 °C in a Joule-Thomson throttling valve and then re-evaporated in the counter-current heat exchanger. The purified CO_2 stream is finally compressed up to 90 bar in a two-stage intercooled compression section and then pumped up to 150 bar to be delivered to the storage site. In this process, a fraction of around 3% of the CO_2 entering the CPU is lost with the vent stream of non-condensable gases. Following the approach proposed by Romano (2013), most of the CO_2 in the vent stream from the CPU can be recovered by feeding the vent gas back to the carbonator of the CaL process (#43).

CaL limestone make-up flow (#8) is introduced though a dedicated limestone mill. Its flow rate is defined through the ratio F_0/F_{CO2}, which indicates the molar flow rate of fresh $CaCO_3$ introduced into the CaL system per mole of CO_2 entering the carbonator with the flue gas. The amount of $CaCO_3$ introduced in the calciner is ultimately extracted as CaO in the CaL purge (#2), cooled to 80 °C (#3) and sent to the raw mill where it is further ground together with additional limestone and correctives (#1) to produce the raw meal (#25). The *integration level* (IL) is therefore defined as the percentage of Ca entering the clinker burning process with the CaL purge with respect to the total Ca fed to the plant.

In the cement kiln integrated with the CaL process, the mass flow rate and composition of the material from the pre-calciner fed to the rotary kiln are kept unchanged with respect to the reference case without CO_2 capture. Therefore, the amount of correctives fed to the raw mill is adjusted taking into account the SiO_2, Fe_2O_3 and Al_2O_3 in the coal ash contained in the CaL purge. The only species that cannot be controlled is $CaSO_4$, which is unavoidably formed in the CaL calciner and the clinker burning line by reaction of CaO with SO_2 generated by coal combustion. Therefore, sulfur content in the final clinker is univocally determined by a mass balance on the total fuel consumption in the plant and increases when the CaL process is used for CO_2 capture compared to the conventional cement plant without CCS. In the reference cement kiln without CO_2 capture, the final clinker contains 0.24%wt. of $CaSO_4$. In the cases assessed in this work, $CaSO_4$ content increases from 0.46%wt. with IL = 80% to 0.95%wt. with IL = 15% when integrating the CaL process. Such $CaSO_4$ concentrations are well below the specification limit for the Portland cement clinker of 2.6%wt. (or 1.5%wt. of SO_3).

In addition to the make-up ratio F_0/F_{CO2}, the sorbent circulation between the carbonator and calciner reactors is another key parameter of the CaL process. This solid circulation is defined through the F_{Ca}/F_{CO2} ratio, which indicates the moles of CaO flowing into the carbonator per mole of CO_2 entering the carbonator with the flue gas. Considering that coal ashes contain significant amount of CaO, only the CaO originating from limestone make-up is considered when computing F_{Ca} (i.e. CaO coming from coal ashes, which may represent up to 5% of total CaO in the cases analyzed in this work, is considered inactive as CO_2 sorbent).

The third CaL main process parameter is the solid inventory in the carbonator. Higher solid inventories lead to higher CO_2 capture rates for given F_0/F_{CO2} and F_{Ca}/F_{CO2} ratios but also to higher gas pressure drops and fan consumption. In this work, an inventory of 1000 kg per m^2 of carbonator cross-section is considered as a baseline value.

The CFB carbonator model developed by Romano (2012) is used for calculating the CO_2 capture efficiency (E_{carb}). This model is based on the Kunii and Levenspiel CFB model (Kunii and Levenspiel, 1997) and considers the kinetic model proposed by Grasa et al. (2008), corrected to take the effect of coal ash and sulphur into account. As a matter of comparison, carbonator efficiency is also calculated assuming that CaO particles achieve their maximum conversion (X_{ave}) in the carbonator. In this ideal situation, E_{carb} is limited either by the equilibrium of the carbonation reaction (i.e. by the equilibrium CO_2 partial pressure in the gas phase at the assumed carbonator temperature) or by the flow of CaO entering the carbonator. This maximum theoretical carbonator capture efficiency can be calculated according to Eq. (2), where X_{ave} is estimated using Eq. (3) considering the semi-empirical CaO capacity decay law proposed by Grasa and Abanades (2006), with a decay constant k of 0.52 and residual capacity X_r of 0.075, and the statistical cycle number distribution r_N calculated by Abanades (2002).

$$E_{carb} = \min\left(\frac{F_{Ca}\cdot X_{ave}}{F_{CO2}}, E_{eq}\right) \tag{2}$$

$$X_{ave} = \sum_{N=1}^{\infty} r_N \cdot \left(\frac{1}{\frac{1}{(1-X_r)} + k\cdot N} + X_r\right) \tag{3}$$

2.3. Heat recovery steam cycle

One of the inherent advantages of the Ca-Looping process is that most of the thermal power generated by coal combustion into the calciner can be efficiently recovered as high temperature waste heat for electricity production. As highlighted by the process flowsheet of Fig. 2, the following heat sources are suitable for heat recovery:

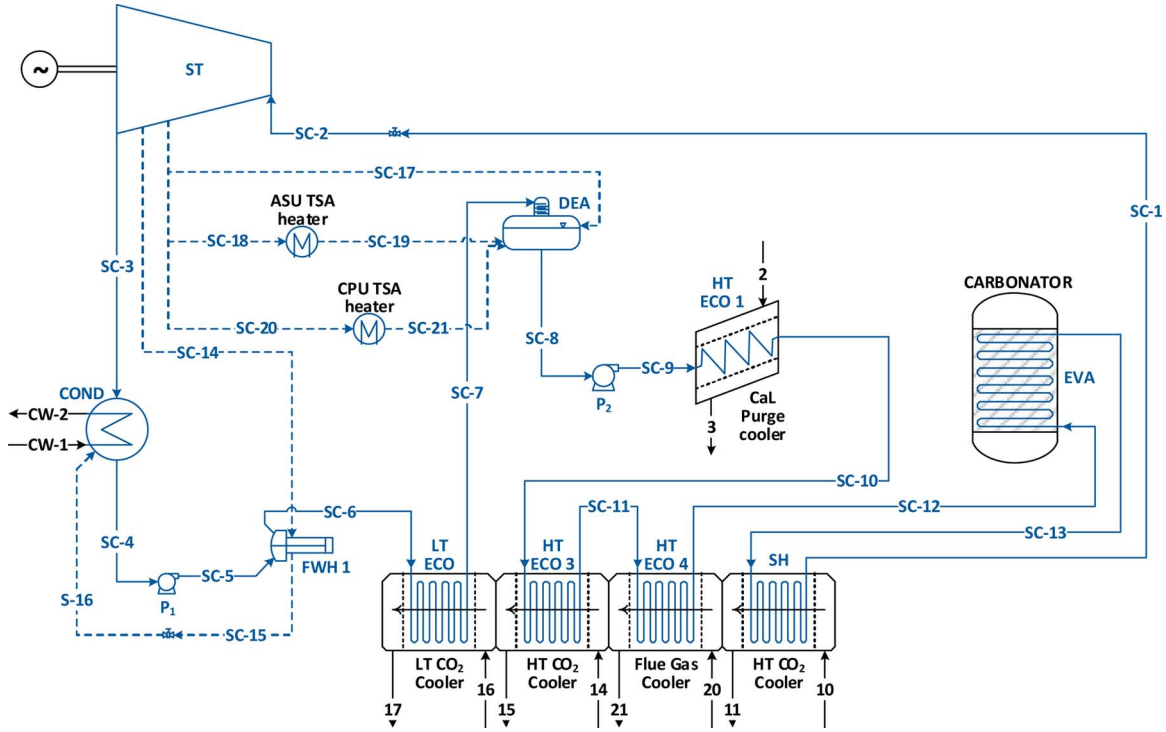

Fig. 3. Process Flow Diagram of the Heat Recovery Steam Cycle (steam cycle streams reported in blue, streams of the CaL process shown in Fig. 2 providing heat to the HRSC reported in black). Properties of the streams of the base case CaL cement kiln with Integration level (IL) = 20%, carbonator solid inventory (Ws) = 1000 kg/m^2 and carbonator efficiency (E_{carb}) = 90% are reported in Table A2 in the Appendix A.

- The 'CARBONATOR', which makes available the carbonation reaction heat and the sensible heat of the circulating solids that are cooled down from the calciner temperature of 920 °C to the carbonator temperature of 650 °C. A separate external heat exchanger could also be used to cool the calcined solids before they enter the carbonator. Such an option will differ in the design of the system, but does not influence the quality of the heat recovered in the process. Therefore, the efficiency of the heat recovery steam cycle and the overall energy performance of the process are not affected by this design variable.
- The flue gases cooler ('*FLUE GAS COOLER*), which extracts thermal power from the CO_2-depleted gaseous stream leaving the carbonator at 650 °C. This gas is cooled down to the temperature that allows providing the heat needed for raw meal drying in the raw mill (about 430 °C for CO_2 capture efficiency in the carbonator of 90%).
- The high and low temperature coolers of the CO_2-rich stream exiting the calciner (*"HT CO2 COOLER 1"*, *'HT CO2 COOLER 2*' and *'LT CO2 COOLER'*), which cool down the gas from calcination temperature to the CPU inlet temperature (80 °C). This cooling section is composed by a sequence of convective heat exchangers. The CO_2-based stream is first cooled to 400 °C (*'HT CO2 COOLER 1'*), before being split into two streams. The first one is recirculated to the calciner, whereas the remaining fraction is further cooled down to 80 °C in two steps (*'HT CO2 COOLER 2'* and '*LT CO2 COOLER*'). Between these two heat exchangers, heat is recovered within the Ca-Looping process for preheating the oxygen stream (#5–6 in Fig. 2) used in the oxy-fuel calciner.
- The purge cooler, which cools the CaO-rich solid purge extracted from the Ca-Looping system down to nearly ambient temperature, before sending it to the raw mill. Here, heat recovery is performed in a fluidized bed cooler where solids are cooled from 920 to 120 °C.

Given both the amount and the temperature level of the waste heat available in the Ca-Looping system, the most efficient and cost-effective technology for electricity production is a Heat Recovery Steam Cycle (HRSC). In this way, it is possible to generate electricity to partly or totally compensate the auxiliary consumption of the cement kiln and of the CO_2 capture section (i.e. the ASU, the CO_2 compression and purification unit, fans, etc.) and in some cases exporting the excess electric power to the grid.

Fig. 3 shows the configuration of the HRSC, whereas Table 1 summarizes the main assumptions adopted for its simulation.

The process flow diagram of the steam cycle is defined by taking into account that, from a thermodynamic point of view, the cycle would benefit from the introduction of regenerative feed-water heating (FWH), since there is a large amount of thermal power available at high temperature (more than 90% of the heat can be recovered above 320 °C), which could be more efficiently exploited for steam evaporation and superheating rather than for economization.

It is worth noting that the choice of the best configuration and set of operating conditions (temperatures and pressures) of the HRSC is driven not only by thermodynamic considerations (e.g., by the T-Q profile of the waste heat available), but also by economic aspects. For instance, the size of the cycle (i.e. the steam turbine power output), which falls in the range 30–85 MW in all the cases herein assessed, as well as the complexity of the heat recovery network, play a significant role in the definition of the best HRSC configuration and steam parameters. Steam cycles with size and complexity similar to the one envisaged in this study are conventional in applications such as waste-to-energy (WTE) plants (Consonni and Viganò, 2012) and biomass-fired and industrial power generation plants (Estabrook and Leger, 2002; Siemens, 2009).

Steam turbine inlet conditions are assumed equal to 100 bar and 530 °C. These parameters are in line with the state of the art of steam turbines, designed for industrial purposes, featuring gross power outputs in the 60–100 MW range (Estabrook and Leger, 2002; Siemens, 2009). This temperature limit allows the adoption of ferritic and low-alloyed steels for the hot sections of the steam cycle, while avoiding the widespread use of expensive materials such as austenitic or high-alloyed steels, typical of large-scale UltraSuperCritical steam cycles for which the adoption of more challenging steam conditions and more complex and highly-efficient layouts is justified by economies of scale (Spliethoff, 2010).

In this paper, the HRSC features a single evaporation level and an air-cooled condenser, where steam is condensed at 0.07 bar. The steam generation section includes two feed-water heaters, i.e. one surface regenerator (FWH 1) and a deaerator operating at 140 °C (DEA). In order to maximize the heat recovery from low-temperature heat sources, a low-temperature economizer (LT ECO) is located between the two preheaters. The liquid exiting the deaerator is first heated through a sequence of coolers where heat from the CaO-rich solid purge, the CO_2-rich calciner exit gas and the CO_2-depleted gas from the carbonator is recovered. Afterwards, the still sub-cooled liquid (SC-12) enters the carbonator, where saturated steam (SC-13) is generated. Finally, steam is superheated to 530 °C (SH) by the high temperature gaseous stream exiting the calciner.

In this work, the relation between the steam turbine size and its isentropic efficiency has been defined according to the curve calibrated by Consonni and Viganò (2012), which reports the variation of the isentropic efficiency as a function of net power output for WTE steam cycles, in the range between 3 and 110 MW. Given the size of the HRSC of interest, the isentropic efficiency of the steam turbine is estimated to be close to 86% and the steam turbine is assumed to be directly connected to the electric generator. The steam cycle conditions are such that the steam quality at the discharge of the steam turbine is always above 88%. The steam turbine features two extractions, the first one at 3.9 bar feeding the deaerator (SC-17) and the ASU and CPU TSA beds (SC-18 and SC-20), whereas the second one (SC-14) feeds the FWH 1 preheater.

Based on economic considerations, steam cycle parameters and steam turbine efficiency may be different from those considered in this work, resulting in a different electric efficiency of the HRSC. The effect of the efficiency of the HRSC on global plant performance has been assessed in Section 4.2.

3. Methodology and key performance indicators

As anticipated, the cement kiln model has been calibrated to

Table 4
Reference efficiency and CO_2 emission factor for power generation technologies. In addition to the power generation technologies proposed in ((CEMCAP (2017), a generic state-of-the-art pulverized coal power plant with CCS is also considered.

Power generation technology	Electric efficiency, %	CO_2 emission factor, kg/MWh
Pulverized coal, state of the art (European Union, 2004)	44.2	770
Pulverized coal, sub-critical	35.0	973
Pulverized coal, state of the art with CCS	35.0	90
Natural gas combined cycle (European Union, 2004)	52.5	385
Renewables (100% efficiency) (IEA, 2015)	100	0

reproduce the heat and mass balances of the reference cement plant of the ECRA and IEAGHG works (Hoenig et al., 2012; IEAGHG, 2013). These balances have been calculated with the proprietary code GS (Gas-Steam cycle), which was developed by the GECOS group of the Department of Energy of Politecnico di Milano (Gecos, 2013). This code assumes ideal behavior for solids, liquids and gases, with thermodynamic properties calculated by means of NASA polynomials (Gardiner, 1984) using thermodynamic databases available in Stull and Prophet (1971). Only pure water/steam is considered as real fluid through the IAPWS 97 thermodynamic properties. The thermodynamic properties of clinker species (C3S, C2S, C3A, C4AF) have been taken from Matschei et al. (2007), while for CaO and $CaCO_3$ properties in Barin (1995) have been used. The validation of the reference cement kiln model is reported in the public Cemcap report "D4.1: Design and performance of CEMCAP cement plant without CO_2 capture" (CEMCAP, 2016). The GS code allows modelling complex processes by means of a modular structure, but it does not have any predictive model for calculating cement kiln components. Therefore, parameters such as the efficiency of the cyclones, calcination degree in the pre-calciner or heat losses in each suspension preheater stage, have been provided as model inputs. The CPU and the steam cycle have been calculated using Aspen Plus. For the CPU, thermodynamic properties of fluids are calculated using the Peng Robinson equation of state, whereas for the HRSC IAPWS-95 is adopted. Finally, the reactor model used for calculating the carbonator of the CaL system has been solved in Matlab.

For evaluating the performance of the cement plant with and without CO_2 capture and for analyzing the effect of the different scenarios and configurations considered in the coming sections, the following key performance indicators are used:

- *Direct fuel consumption* (q) [MJ_{LHV}/t_{clk}], which indicates the primary energy consumed through coal combustion in the cement plant (i.e. rotary kiln, pre-calciner and CaL calciner) per unit of clinker produced.
- *Indirect fuel consumption* (q_e) [MJ_{LHV}/t_{clk}], which indicates the primary energy consumption associated to the net electric consumption in the cement plant (P_e) and it is calculated according to Eq. (4). Based on this definition, when electricity is exported from the cement plant to the grid, as in most of the CaL cases in this paper, q_e becomes negative, indicating a credit of primary energy.

$$q_e = \frac{P_e}{\eta_{ref,e}} \tag{4}$$

The calculation of the indirect fuel consumption needs the definition of a reference electric efficiency ($\eta_{ref,e}$), which depends on the fuel and technology used for generating the electricity consumed in the cement kiln. Coherently with CEMCAP (2017), different electricity production scenarios are considered in this work, as shown in Table 4.

- *Equivalent fuel consumption* (q_{eq}) [MJ_{LHV}/t_{clk}], which is the sum of the direct (q) and indirect (q_e) fuel consumptions defined above.
- *Direct CO_2emissions* (e_{CO2}) [kg_{CO2}/t_{clk}], which refer to the amount of CO_2 directly emitted at the stack of the cement plant to the atmosphere per unit of clinker produced.
- *Indirect CO_2emissions* ($e_{CO2,e}$) [kg_{CO2}/t_{clk}], which correspond to the CO_2 emissions associated to the production of the electricity consumed in the full process P_e. These indirect emissions are calculated according to Eq. (5), where the term $e_{ref,e}$ refers to the specific emissions of the reference electric scenario considered (i.e. those reported in Table 4). In case of electricity export to the grid (i.e. $P_e < 0$), the indirect emissions are negative, indicating a CO_2 emission credit.

$$e_{CO2,e} = P_e \cdot e_{ref,e} \tag{5}$$

- *Equivalent CO_2emissions* ($e_{CO2,eq}$) [kg_{CO2}/t_{clk}], which are the total CO_2 emissions, defined as the sum of the direct (e_{CO2}) and the indirect ($e_{CO2,e}$) emissions.
- *Specific Primary Energy Consumption for CO_2Avoided (SPECCA)* [MJ_{LHV}/kg_{CO2}], which is calculated by Eq. (6), indicates the additional equivalent primary energy consumption to avoid the emission of a unit mass of equivalent CO_2 with respect to the reference cement kiln without CO_2 capture.

$$SPECCA = \frac{q_{eq} - q_{eq-ref}}{e_{CO2,eq-ref} - e_{CO2,eq}} \tag{6}$$

4. Results

Fig. 4 shows the CO_2 capture efficiency attained in the carbonator of the CaL system as a function of the F_{Ca}/F_{CO2} ratio for ILs of 15, 20 and 25%, which correspond to F_0/F_{CO2} values of 0.11, 0.16 and 0.21,

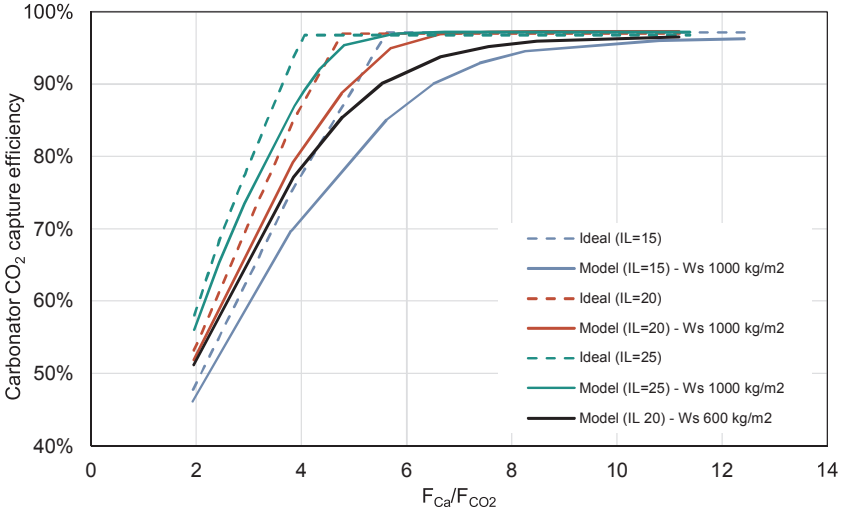

Fig. 4. Carbonator CO_2 capture efficiency as a function of the F_{Ca}/F_{CO2} ratio and the integration level IL, as predicted by the carbonator model of Romano (2012), for inventories of 1000 and 600 kg/m^2 (solid lines), compared with the ideal capture rate given by Eqs. (2) and (3) (dashed lines).

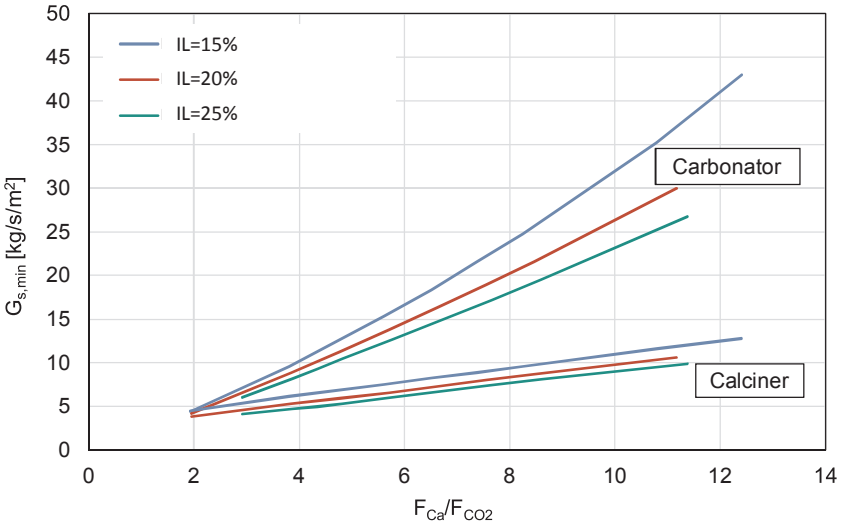

Fig. 5. Minimum solid circulation in the reactors of the CaL system as a function of the Integration Level (IL) and the CaO circulation rate (F_{Ca}/F_{CO2}).

respectively. Capture efficiency curves calculated by the reactor model developed by Romano (2012) are compared with the ideal capture rate calculated by Eqs. (2)–(3).

High ILs lead to high sorbent make-up in the CaL process and therefore to highly active CaO sorbent in the CaL reactor system, which results in an increase of the carbon capture efficiencies achieved in the carbonator. As can be seen in Fig. 4, two regions can be distinguished for all the curves. For low values of the sorbent circulation rate F_{Ca}/F_{CO2}, the CO_2 capture efficiency in the carbonator (E_{carb}) is limited by the availability of active sorbent in this reactor, and a steep E_{carb} increase can be observed when solid circulation is raised. For high values of F_{Ca}/F_{CO2}, the capture efficiency E_{carb} is limited by the thermodynamic equilibrium of the carbonation reaction and the maximum theoretical capture efficiency of about 96% is achieved in the ideal case, which is asymptotically approached when the reactor model is used. For the ideal cases, a sharp transition between the two zones is appreciated, whereas for the cases calculated using the carbonator model a smooth transition is noticed, indicating that carbonator performance is limited by kinetics and mass transport when active sorbent circulation is close to the stoichiometric one.

Concerning the IL between the CaL system and the cement plant, when increasing the sorbent make-up flow into the CaL system, the amount of solids purged from the system increases, reducing the amount of ashes from coal and $CaSO_4$ in the solid population and the average number of calcination-carbonation cycles experienced by CaO particles. Both effects favor the average reactivity of the solids population, which leads to a smaller difference between the ideal and the model curves. Moreover, the increase of the average CaO activity for higher ILs shifts the transition between the two aforementioned zones to lower values of the F_{Ca}/F_{CO2} ratio.

Another aspect to take into account about the IL between the CaL system and the cement plant concerns the increase of inert species (i.e. ashes and $CaSO_4$) in the solid purge sent to the cement kiln. When reducing the F_0/F_{CO2} in the CaL process, the buildup of inert material in this process increases, resulting in a higher content of these species in the CaO-rich purge sent to the raw mill. Concerning the $CaSO_4$, as anticipated in Section 2.2, its weight fraction in the final clinker produced reaches the maximum value of 0.95%wt. for the most unfavorable set of conditions shown in Fig. 4 (i.e. minimum IL of 15% and largest solid circulation between reactors, $F_{Ca}/F_{CO2} > 12$).

For the sake of comparison, a case with a reduced solid inventory in the carbonator is also reported in Fig. 4 for IL of 20%. When diminishing the solid inventory in the carbonator from the initial 1000 kg/m^2 to 600 kg/m^2, the CO_2 capture efficiency in this reactor diminishes due to the reduced active space time (Charitos et al., 2011; Romano, 2012). The highest effect is again in the transition zone between the chemical equilibrium-limited and the sorbent availability-limited zones, where the effect of kinetics on CO_2 capture efficiency is higher.

As far as the fluidized beds hydrodynamics is concerned, the minimum specific solid flow rate per unit of fluidized bed cross section ($G_{s,min}$) needed to ensure solids circulation between the two reactors has been calculated. For both the carbonator and the calciner, the reactors cross section is computed by assuming a gas superficial velocity of 5 m/s. $G_{s,min}$ is therefore computed as the ratio between the mass flow rate of the solids flowing between the reactors and the cross-section of the reactor where such solids come from. Fig. 5 shows $G_{s,min}$ as a function of IL and F_{Ca}/F_{CO2}. For F_{Ca}/F_{CO2} ratios in the CaL system between 4 and 6, minimum solid circulations are in the range of 8–17 kg/m^2 s and of 4–7 kg/m^2 s for the carbonator and the calciner respectively. These values of $G_{s,min}$ are in the range of the typical solid circulation of commercial CFB combustors, indicating that the solid circulation can be entirely sustained by the transport capacity of the gas in the reactors. As can be seen from Fig. 4, at F_{Ca}/F_{CO2} of 4–6, carbon capture efficiencies between 70% and > 95% are feasible in the carbonator of the CaL system depending on the IL.

Detailed results of the heat and mass balances are shown in Table 5 for selected cases with IL between 15 and 80%, Ws of 1000 and 600 kg/m^2 and solids circulation rates adjusted to achieve E_{carb} of 90% (from second to fifth column). For the sake of comparison, results obtained for the reference cement kiln without CO_2 capture have been also included in this table (first column).

The total fuel thermal input increases by 95–210% when including the CaL into the cement plant. Fuel consumption in the rotary kiln remains basically constant, while fuel consumption in the pre-calciner reduces by 17% for IL = 15% to 93% for IL = 80% with respect to the reference cement kiln, because of the replacement of $CaCO_3$ in the raw meal with CaO from the CaL solid purge. Consequently, the higher the IL, the lower the fuel consumption in the pre-calciner. Regarding fuel consumption in the calciner of the CaL process, it accounts for about 70–80% of the total fuel consumption of the plant, which corresponds

Table 5
Main results from the heat and mass balances of cement kilns integrated with the CaL system with different operating parameters and of the benchmark cement kiln without CO_2 capture.

	Cement plant w/o CCS		Case IL15-W1000		Case IL20-W1000		Case IL25-W1000		Case IL50-W1000		Case IL80-W1000		Case IL20-W600		Case IL20-W1000-VentRec	
IL, %		–	15		20		25		50		80		20		20	
F_0/F_{CO2}		–	0.11		0.16		0.21		0.60		1.84		0.16		0.15	
F_{Ca}/F_{CO2}		–	6.51		4.78		4.35		2.94		3.23		5.53		5.32	
Carbonator inventory, kg/m^2		–	1000		1000		1000		1000		1000		600		1000	
Total heat Input (q), MW_{LHV} – MJ_{LHV}/kg_{clk}	105.4	3.22	328.2	10.00	284.3	8.67	274.3	8.37	230.9	7.06	205.2	6.26	296.2	9.03	305.1	9.30
Heat Input, rotary kiln, MW_{LHV} – MJ_{LHV}/kg_{clk}	40.0	1.22	39.7	1.21	39.7	1.21	39.7	1.21	39.7	1.21	39.7	1.21	39.7	1.21	39.7	1.21
Heat Input, pre-calciner, MW_{LHV} – MJ_{LHV}/kg_{clk}	65.3	2.00	54.4	1.66	50.6	1.54	46.7	1.43	27.5	0.84	4.4	0.14	50.6	1.54	50.6	1.54
Heat Input, Ca-Looping calciner, MW_{LHV} – MJ_{LHV}/kg_{clk}	–	–	234.2	7.13	194.1	5.92	187.9	5.73	163.7	5.01	161.1	4.91	205.9	6.28	214.8	6.55
Oxygen Input, t/day – kg_{O2}/kg_{clk}	–	–	1738.8	0.61	1453.9	0.51	1411.8	0.50	1236.2	0.44	1214.1	0.43	1538.6	0.54	1605.9	0.57
Power balance																
Gross steam turbine electricity production, MW_e – kWh_e/t_{clk}	–	–	84.36	713.8	66.16	560.6	61.82	524.0	41.58	353.2	30.79	262.1	71.01	601.5	75.65	640.7
Steam cycle pumps, MW_e – kWh_e/t_{clk}	–	–	−1.62	−13.7	−1.28	−10.9	−1.20	−10.2	−0.80	−6.8	−0.595	−5.1	−1.34	−11.4	−1.43	−12.1
Auxiliaries for steam cycle heat rejection, MW_e – kWh_e/t_{clk}	–	–	−1.38	−11.7	−1.11	−9.4	−1.05	−8.9	−0.78	−6.6	−0.601	−5.1	−1.18	−10.0	−1.25	−10.6
ASU consumption, MW_e – kWh_e/t_{clk}	–	–	−16.36	−138.5	−13.75	−116.5	−13.37	−113.3	−11.80	−100.2	−11.60	−98.7	−14.52	−123.0	−15.13	−128.1
Carbonator fan, MW_e – kWh_e/t_{clk}	–	–	−1.70	−14.4	−1.68	−14.2	−1.66	−14.0	−1.55	−13.2	−1.43	−12.2	−1.10	−9.3	−1.14	−9.7
CO_2 recycle fan, MW_e – kWh_e/t_{clk}	–	–	−0.88	−7.5	−0.74	−6.3	−0.72	−6.1	−0.63	−5.3	−0.62	−5.3	−0.78	−6.6	−1.14	−9.7
CO_2 compression, MW_e – kWh_e/t_{clk}	–	–	−19.32	−163.5	−17.59	−149.0	−17.58	−149.0	−16.06	−136.5	−15.49	−131.9	−18.17	−153.9	−19.04	−161.3
Auxiliaries for calciner fuel grinding, MW_e – kWh_e/t_{clk}	–	–	−0.26	−2.2	−0.22	−1.8	−0.21	−1.8	−0.18	−1.5	−0.18	−1.5	−0.23	−1.9	−0.24	−2.0
Cement plant auxiliaries, MW_e – kWh_e/t_{clk}	−15.49	−131.6	−15.55	−131.6	−15.53	−131.6	−15.53	−131.6	−15.49	−131.6	−15.46	−131.6	−15.54	−131.6	−15.54	−131.6
Net electricity production (P_e), MW_e – kWh_e/t_{clk}	−15.49	−131.6	27.28	230.8	14.27	120.9	10.51	89.1	−5.72	−48.6	−15.19	−129.3	18.15	153.8	20.73	175.6
Net electricity production (P_e), kWh_e/t_{cem}	−97.0		170.1		89.1		65.7		−35.8		−95.3		113.3		129.4	

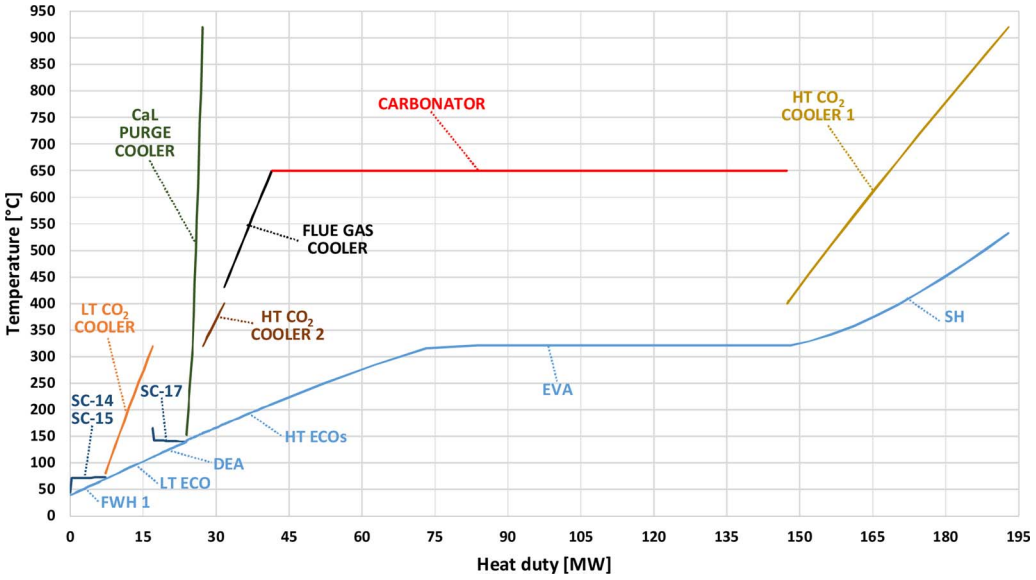

Fig. 6. T-Q cumulative diagram for the heat recovered from CaL streams for the base case with IL = 20%, Ws = 1000 kg/m^2 and E_{carb} = 90%.

to 150–220% of the fuel consumption in the reference cement plant without capture. The reason for such a large increase of fuel consumption is intrinsic in the tail-end configuration (see Fig. 1), because the CO_2 released in the pre-calciner from the raw meal calcination results in the formation of $CaCO_3$ in the carbonator of the CaL process, which is calcined again in the oxyfuel calciner. This double calcination step, needed for capturing the molecules of CO_2 originally in the limestone fed to the pre-calciner of the cement kiln, involves significant overall fuel consumption. This double calcination effect reduces if IL increases because limestone fed to the CaL calciner is subject to a single oxyfuel calcination process. This is why the lowest overall fuel consumption has been obtained for the case with IL = 80%.

Concerning the electric power balance of the selected cases shown in Table 5, the main electric consumptions are due to oxygen production in the ASU and to CO_2 compression. In the cases with IL between 15 and 25%, electricity produced by the steam cycle exceeds the electricity consumed by these process units and the other auxiliaries, resulting in a net power export between 65 and 170 kWh/t_{cem}, to be compared with the net electricity import of 97 kWh/t_{cem} of the reference cement plant without CO_2 capture. For the cases with IL of 50 and 80%, net power import between 36 and 95 kWh/t_{cem} is obtained. Therefore, in the case with IL = 80%, the power generated by the steam cycle compensates the consumptions of the ASU, CPU and other auxiliaries, resulting in a net electric balance very similar to the benchmark plant without CO_2 capture. In general, higher power export is obtained by lowering the IL, because of the increase of the fuel input to the CaL and the consequently higher thermal power available for the steam cycle.

The result of the case where the CO_2-rich vent gas from the CPU is recycled to the carbonator is shown in the last column of Table 5 for the case with IL = 20%. Increased fuel consumption by 10.7% in the CaL calciner is obtained with respect to the corresponding case without vent recycle and the same IL and inventory, due to the increased CO_2 flow rate captured in the carbonator. This is because the target carbonator efficiency of 90% here includes also the CO_2 flow contained in the CPU off gas. As a consequence of the higher fuel consumption, electricity produced by the steam cycle is also higher, with a net electricity export of 129 kWh/t_{cem}, which is about 45% higher than in the corresponding case without CPU vent recycle.

Fig. 6 shows the cumulative Temperature-Heat duty curve for the HRSC of the selected case with IL = 20%. As noticed, most of the thermal input to the steam cycle is provided by the carbonator of the CaL process, which in this case makes available about 105 MW compared to an overall thermal power input of 179 MW to the HRSC. It is worth highlighting that the pinch point occurs at the entrance of the high temperature economizer HT ECO1 and the low temperature economizer LT ECO (i.e. between streams SC-9 and 3 and between SC-6 and 17 of Fig. 3), whereas larger temperature differences (always higher than 50 °C) occur in the other economizers, and in the evaporation and superheating sections.

In the cases shown in Table 5, the steam cycle achieves net electric efficiencies (i.e. net electric power output divided by the thermal power provided to the steam cycle) of about 35%. Slightly higher efficiencies are obtained for the cases with higher fuel input, mainly because of the higher fraction of heat available at high temperature.

As anticipated before, indirect fuel consumption and CO_2 emissions have been evaluated with respect to different reference electric production scenarios. Depending on the scenario considered, values of the electric production efficiency ($\eta_{ref,e}$) and the specific emissions ($e_{ref,e}$) change. From a technical point of view, the authors consider the state-of-the-art coal-fired ultra-supercritical (USC) power plant as the most reasonable reference power generation scenario, because it represents the state-of-the-art power generation technology using the same type of fuel of the cement plant. On the other hand, from a Life Cycle Assessment (LCA) perspective, the actual indirect emissions and fuel consumptions of a CCS project will depend on the specific technology that will balance the variation of the power exchanged with the grid, which is very much dependent on the installation site. In Table 6, key performance indicators are computed considering the four mentioned scenarios for electricity production indicated in Table 4.

Direct CO_2 emissions in the selected cases with different ILs are reduced by 86–94% with respect to the cement plant without CCS. Highest direct CO_2 emissions correspond to the lowest IL case because this is the case with the largest amount of CO_2 generated in the CaL calciner (i.e. largest fuel consumption in this reactor as given in Table 5), and therefore the largest amount of CO_2 lost with non-condensable species from the CPU. In the case with CPU vent recycle to the carbonator, direct emission reduction of 91.5% is obtained.

Table 6
Key performance indicators for the selected cases with different IL under different reference scenarios for electricity production.

	Cement plant w/o CCS		Case IL15-W1000		Case IL20-W1000		Case IL25-W1000		Case IL50-W1000		Case IL80-W1000		Case IL20-W600		Case IL20-W1000-VentRec	
Direct fuel consumption (q), MW_{LHV} – MJ_{LHV}/kg_{clk}	105.4	3.22	328.2	10.00	284.3	8.67	296.2	9.03	230.9	7.06	205.2	6.29	296.2	9.03	305.1	9.30
Direct CO_2 emission (e_{CO2}), kg/s – kg_{CO2}/t_{clk}	28.3	865.2	4.0	120.4	3.9	117.7	3.6	110.5	2.5	76.3	1.7	52.7	3.6	110.5	2.4	73.1
Direct emission reduction, %	–		85.9%		86.2%		89.8%		91.2%		93.9%		87.3%		91.5%	
State of the art pulverized coal ultra-supercritical power plant (η_e = 44.20%, E_{CO2} = 770 kg_{CO2}/MWh_e)																
Indirect fuel consumption (q_e), MW_{LHV} – MJ_{LHV}/kg_{clk}	35.0	8.98	−61.7	−1.88	−32.3	−0.99	−23.8	−0.73	12.9	0.39	34.4	1.05	−41.1	−1.25	−46.9	−1.43
Equivalent fuel consumption (q_{eq}), MW_{LHV} – MJ_{LHV}/kg_{clk}	140.4	4.30	266.5	8.12	252.0	7.69	250.5	7.64	243.8	7.45	239.6	7.34	255.1	7.78	258.2	7.87
Indirect CO_2 emission ($e_{CO2,e}$), kg/s – kg_{CO2}/t_{clk}	3.3	101.3	−5.8	−177.7	−3.1	−93.1	−2.2	−68.6	1.2	37.2	3.2	99.6	−3.9	−118.4	−4.4	−135.2
Equivalent CO_2 emission ($e_{CO2,eq}$), kg/s- kg_{CO2}/t_{clk}	31.6	966.6	−1.9	−57.3	0.8	24.5	0.7	21.3	3.7	113.5	5.0	152.3	−0.3	−7.9	−2.0	−62.1
Equivalent fuel consumption increase, %	–		89.8%		79.5%		78.4%		73.6%		70.7%		81.7%		83.9%	
Equivalent emission reduction, %	–		−106.0%		−97.5%		−97.8%		−88.3%		−84.3%		−100.8%		−106.4%	
SPECCA, MJ_{LHV}/kg_{CO2}	–		3.74		3.60		3.54		3.70		3.74		3.57		3.48	
Pulverized coal subcritical power plant (η_e = 35.0%, E_{CO2} = 973 kg_{CO2}/MWh_e)																
Indirect fuel consumption (q_e), MW_{LHV} – MJ_{LHV}/kg_{clk}	44.3	11.34	−77.9	−2.37	−40.8	−1.24	−30.0	−0.92	16.3	0.50	43.4	1.33	−51.9	−1.58	−59.2	−1.81
Equivalent fuel consumption (q_{eq}), MW_{LHV} – MJ_{LHV}/kg_{clk}	149.6	4.58	250.3	7.63	243.5	7.43	244.2	7.45	247.1	7.56	248.6	7.62	244.3	7.45	245.8	7.49
Indirect CO_2 emission ($e_{CO2,e}$), kg/s – kg_{CO2}/t_{clk}	4.2	128.1	−7.4	−224.6	−3.9	−117.7	−2.8	−86.7	1.5	47.0	4.1	125.8	−4.9	−149.6	−5.6	−170.8
Equivalent CO_2 emission ($e_{CO2,eq}$), kg/s- kg_{CO2}/t_{clk}	32.5	993.3	−3.4	−104.2	0.0	0.0	0.1	3.2	4.0	123.3	5.8	178.5	−1.3	−39.1	−3.2	−97.7
Equivalent fuel consumption increase, %	–		67.3%		62.8%		63.2%		65.2%		66.2%		63.3%		64.3%	
Equivalent emission reduction, %	–		−110.5%		−100.0%		−99.7%		−87.6%		−82.1%		−103.9%		−109.9%	
SPECCA, MJ_{LHV}/kg_{CO2}	–		2.78		2.87		2.90		3.43		3.73		2.78		2.67	
Pulverized coal power plant with CCS (η_e = 35.0%, E_{CO2} = 90 kg_{CO2}/MWh_e)																
Indirect fuel consumption (q_e), MW_{LHV} – MJ_{LHV}/kg_{clk}	44.3	11.34	−77.9	−2.37	−40.8	−1.24	−30.0	−0.92	16.3	0.50	43.4	1.33	−51.9	−1.58	−59.2	−1.81
Equivalent fuel consumption (q_{eq}), MW_{LHV} — MJ_{LHV}/kg_{clk}	149.6	4.58	250.3	7.63	243.5	7.43	244.2	7.45	247.1	7.56	248.6	7.62	244.3	7.45	245.8	7.49
Indirect CO_2 emission ($e_{CO2,e}$), kg/s – kg_{CO2}/t_{clk}	0.39	11.8	−0.7	−20.8	−0.4	−10.9	−0.3	−8.0	0.1	4.4	0.4	11.6	−0.5	−13.8	−0.5	−15.8
Equivalent CO_2 emission ($e_{CO2,eq}$), kg/s- kg_{CO2}/t_{clk}	28.7	877.1	3.3	99.6	3.5	106.8	2.7	81.9	2.6	80.6	2.1	64.4	3.2	96.7	1.9	57.3
Equivalent fuel consumption increase, %	–		67.3%		62.8%		63.2%		65.2%		66.2%		63.3%		64.3%	
Equivalent emission reduction, %	–		−88.6%		−87.8%		−90.6%		−90.8%		−92.7%		−88.9%		−93.4%	
SPECCA, MJ_{LHV}/kg_{CO2}	–		3.92		3.70		3.62		3.74		3.74		3.68		3.56	
State of the art natural gas combined cycle (η_e = 52.5%, E_{CO2} = 385 kg_{CO2}/MWh_e)																
Indirect fuel consumption (q_e), MW_{LHV} – MJ_{LHV}/kg_{clk}	29.5	7.56	−52.0	−1.58	−27.2	−0.83	−20.0	−0.61	10.8	0.33	28.9	0.89	−34.6	−1.05	−39.5	−1.20
Equivalent fuel consumption (q_{eq}), MW_{LHV} – MJ_{LHV}/kg_{clk}	134.9	4.13	276.3	8.42	257.1	7.84	254.2	7.76	241.7	7.39	234.2	7.18	261.6	7.98	265.6	8.10
Indirect CO_2 emission ($e_{CO2,e}$), kg/s – kg_{CO2}/t_{clk}	1.7	50.7	−2.9	−88.9	−1.5	−46.6	−1.1	−34.3	0.6	18.6	1.6	49.8	−1.9	−59.2	−2.2	−67.6
Equivalent CO_2 emission ($e_{CO2,eq}$), kg/s- kg_{CO2}/t_{clk}	29.9	915.9	1.0	31.6	2.3	71.1	1.8	55.6	3.1	94.9	3.3	102.5	1.7	51.3	0.2	5.5
Equivalent fuel consumption increase, %	–		104.9%		90.7%		88.5%		79.2%		73.6%		94.0%		96.9%	
Equivalent emission reduction, %	–		−96.5%		−92.2%		−93.9%		−89.6%		−88.8%		−94.4%		−99.4%	
SPECCA, MJ_{LHV}/kg_{CO2}	–		4.85		4.40		4.22		3.98		3.75		4.45		4.36	
Renewable energy (η_e = 100%, E_{CO2} = 0 kg_{CO2}/MWh_e)																
Indirect fuel consumption (q_e), MW_{LHV} – MJ_{LHV}/kg_{clk}	15.5	3.97	−27.3	−0.83	−14.3	−0.44	−10.5	−0.32	5.7	0.17	15.2	0.47	−18.2	−0.55	−20.7	−0.63

(*continued on next page*)

Table 6 (*continued*)

	Cement plant w/o CCS		Case IL15-W1000		Case IL20-W1000		Case IL25-W1000		Case IL50-W1000		Case IL80-W1000		Case IL20-W600		Case IL20-W1000-VentRec	
Equivalent fuel consumption (q_{eq}), MW_{LHV} – MJ_{LHV}/kg_{clk}	120.8	3.70	301.0	9.17	270.1	8.24	263.7	8.05	236.6	7.24	220.4	6.75	278.0	8.48	284.3	8.67
Indirect CO_2 emission ($e_{CO2,e}$), kg/s – kg_{CO2}/t_{clk}	0.0	0.0	0.0	0.0	0.0	0.0	0.0	0.0	0.0	0.0	0.0	0.0	0.0	0.0	0.0	0.0
Equivalent CO_2 emission ($e_{CO2,eq}$), kg/s- kg_{CO2}/t_{clk}	28.3	865.2	4.0	120.4	3.9	117.7	2.9	89.9	2.5	76.3	1.7	52.7	3.6	110.5	2.4	73.1
Equivalent fuel consumption increase, %	–		149.0%		123.5%		118.2%		95.8%		82.4%		130.0%		135.3%	
Equivalent emission reduction, %	–		−86.0%		−86.4%		−89.6%		−91.2%		−93.9%		−87.2%		−91.5%	
SPECCA, MJ_{LHV}/kg_{CO2}	–		7.35		6.07		5.61		4.48		3.76		6.33		6.28	

As noticed in Table 6, for the three scenarios with electric power generation by fossil fuels, negative indirect CO_2 emissions are obtained for the cases with IL = 15–25%, as a consequence of the export of electricity to the grid (i.e. $P_e < 0$ in Eq. (5)). For the coal-based power generation without CCS scenarios, emission credits are such that equivalent CO_2 emissions approach zero and become even negative for the case with IL = 15%, leading to equivalent emission reductions higher than 100%. For the cases with higher IL, positive indirect emissions are obtained, leading to percentage equivalent emission reduction lower than direct emission reduction. In the renewable power generation scenario, there are no indirect emissions associated to the import/export of electricity and equivalent CO_2 emissions are equal to the direct CO_2 emissions of the cement plant with CCS. In the intermediate case with natural gas-based power generation scenario, equivalent emission reduction between 89 and 100% are obtained.

As to the SPECCA, a wide range of values is obtained, as shown in Table 6, mainly depending on the reference power generation scenario considered. For coal-based power generation scenario, SPECCA of 2.7-3.7 MJ/kg and 3.5-3.7 MJ/kg have been obtained for the subcritical and ultra-supercritical reference technologies, respectively, which are values comparable to the SPECCA of benchmark CO_2 capture technologies integrated in coal-fired power plants, calculated with consistent methodology (EBTF, 2011; Kvamsdal et al., 2014; Romano, 2013). For coal-based power generation with CCS scenario, SPECCA between 3.6 and 3.9 MJ/kg have been obtained, i.e. slightly higher than the PC supercritical plant without capture. SPECCA increases in the renewable power generation scenario, up to 3.8-7.4 MJ/kg, and in the natural gas power generation scenario, up to 3.8-4.9 MJ/kg. These results highlight the significant influence of the CO_2 intensity of the electricity mix on the SPECCA index and therefore on the attractiveness of the CaL process, from the energy and environmental perspective. The only case whose SPECCA is unaffected by the power generation scenario is the case with IL = 80%. In this case the net electric consumption is very close to the reference cement plant without capture. Therefore, indirect emissions and fuel consumptions are virtually the same, independently of the power generation scenario considered.

4.1. Retrofittability

In this section, the retrofittability of the CaL process in existing cement kilns is discussed. In Fig. 7, the solid/gas mass ratio and the gas flow rate along the preheating tower of the reference cement kiln and of the CaL cement kiln with IL = 20%, Ws = 1000 kg/m^2 and E_{carb} = 90% are compared. Gas volume flow rate (and therefore gas velocity) decreases by 3–4% in the CaL case, because the replacement of part of the $CaCO_3$ in the raw meal with the CaO-rich solids purged from the CaL system results in a lower fuel thermal input in the pre-calciner and in a lower amount of CO_2 released from raw meal calcination. On the other hand, the mass flow rate of solids introduced in the tower is also reduced due to the partial substitution of $CaCO_3$ with CaO. As a consequence, the solid/gas mass ratio along the pre-heating tower barely changes with respect to the reference cement kiln without CO_2 capture.

When the integration level is increased to 50% and 80%, gas volume flow rate in the preheating tower reduces to 8–10% and 14–17% respectively. The stable operation of the preheating tower has to be verified in these cases and the reduction of the inner diameter of the risers (e.g. by increasing the thickness of the refractory) or the increase of the gas flow rate through excess air blowing may be needed to ensure proper lifting of the solids. On the other hand, the reduction of the gas flow rate in the preheating tower could also provide the opportunity of increasing the productivity of the cement kiln, increasing the gas flow rate by increasing the clinker production. The flexibility of the existing equipment, especially of the clinker cooler, in accommodating a larger clinker production should be verified in this case.

Fig. 8 compares the temperature-heat diagrams in the pre-heating

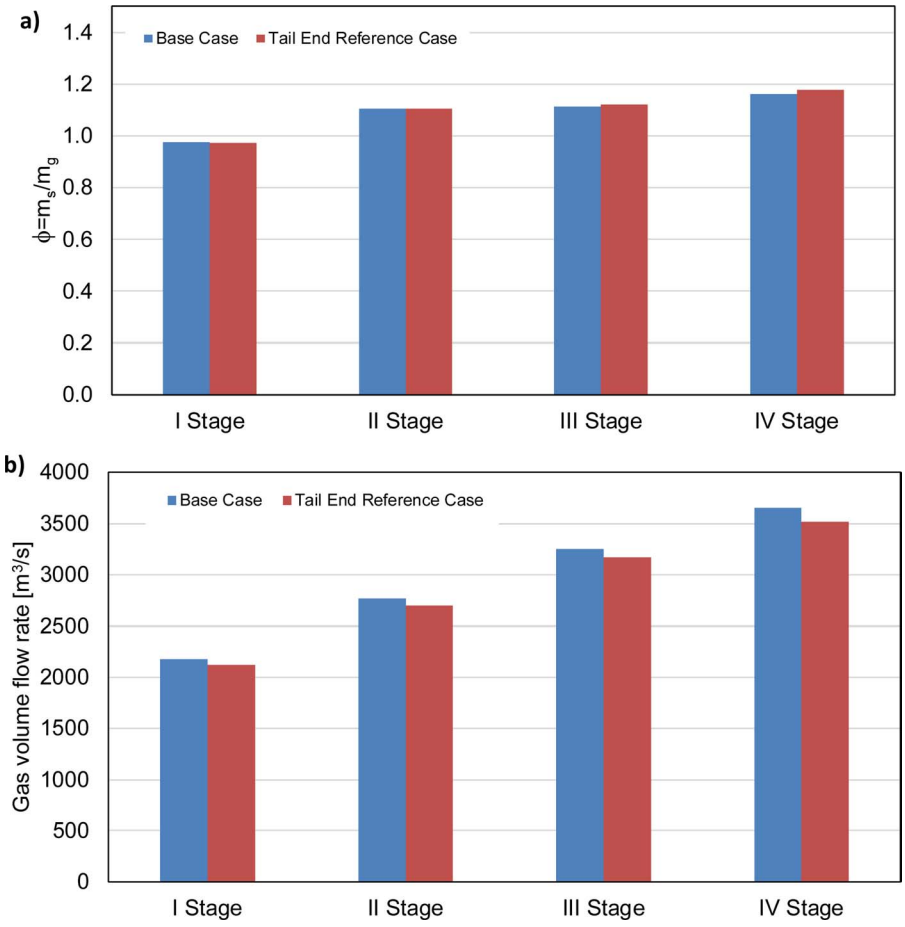

Fig. 7. Solid/gas mass ratio (a) and gas volume flow rate (b) at the outlet of each stage of the preheating tower of the cement kiln without CO_2 capture (Base Case) and of the cement kiln with CaL process and IL = 20% (Tail End Reference Case).

tower of the reference cement kiln without CO_2 capture and of the CaL kiln. In the CaL case, the total heat exchanged reduces by 15% due to the reduced heat capacities of both the solid and gas streams in the tower. Temperatures at the outlet of each stage increase by 10–20 °C. However, despite of these differences, the final temperature reached by the solids at the inlet of the pre-calciner is practically the same (750 °C vs. 761 °C).

Based on the results shown in Figs. 7 and 8, it can be concluded that the performance of the exiting equipment will not be altered when integrating a tail-end CaL system and retrofitting of an existing cement kiln is possible with no modifications of the preheating tower in case of low ILs.

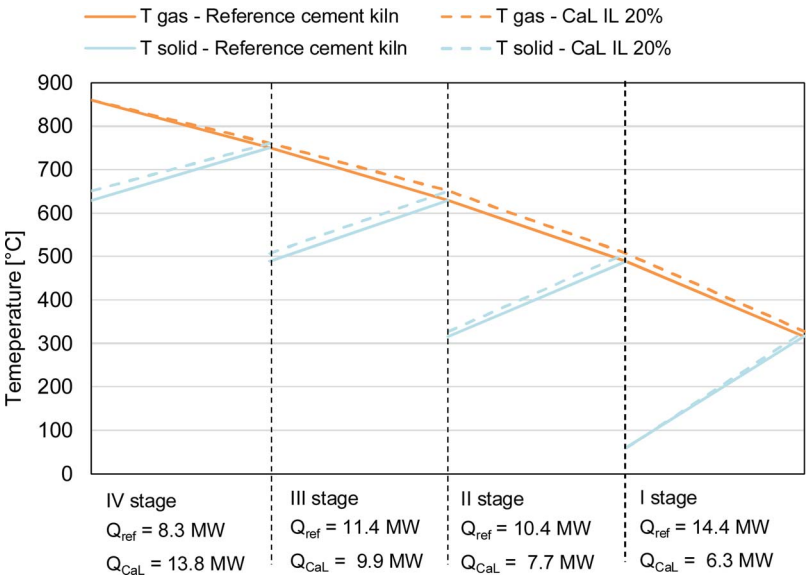

Fig. 8. Temperature profiles and heat exchanged in the preheating tower of the reference cement kiln without capture (solid lines) and of the cement kiln with CaL process and IL = 20% (dashed lines).

Table 7
Main results of the CaL cement kiln with IL = 20%, Ws = 1000 kg/m^2 and E_{carb} = 90%, for the base case shown in Fig. 2 with the carbonator placed before the raw mill and for a case with the carbonator placed after the raw mill.

	Carbonator before the raw mill		Carbonator after the raw mill	
F_0/F_{CO2}	0.16		0.16	
F_{Ca}/F_{CO2}	4.78		4.97	
Gas volume flow rate at carbonator inlet, Nm^3/s – Nm^3/kg_{clk}	42.9	1.31	73.1	2.23
Total heat Input, MW_{LHV} – MJ_{LHV}/kg_{clk}	284.3	8.67	286.0	8.72
Heat Input, rotary kiln, MW_{LHV} – MJ_{LHV}/kg_{clk}	39.7	1.21	39.7	1.21
Heat Input, pre-calciner, MW_{LHV} – MJ_{LHV}/kg_{clk}	50.6	1.54	50.6	1.54
Heat Input, Ca-Looping calciner, MW_{LHV} – MJ_{LHV}/kg_{clk}	194.1	5.92	195.8	5.97
Power balance				
Gross steam turbine electricity production, MW_e – kWh_e/t_{clk}	66.16	560.6	65.73	557.0
Steam cycle pumps and auxiliaries, MW_e – kWh_e/t_{clk}	−2.39	−20.2	−2.35	−19.9
Other auxiliaries, MW_e – kWh_e/t_{clk}	−49.50	−419.4	−49.81	−422.1
Net electricity production (P_e), MW_e – kWh_e/t_{clk}	14.27	120.9	13.57	115.0
Net electricity production (P_e), kWh_e/t_{cem}	89.1		84.8	
State of the art pulverized coal ultra-supercritical power plant (η_e = 44.20% and 770 g_{CO2}/kWh_e)				
Equivalent fuel consumption (q_{eq}), MW_{LHV} – MJ_{LHV}/kg_{clk}	252.0	7.69	255.3	7.79
Direct CO_2 emission (e_{CO2}), kg/s – kg_{CO2}/t_{clk}	3.9	117.7	4.0	123.3
Equivalent CO_2 emission ($e_{CO2,eq}$), kg/s – kg_{CO2}/t_{clk}	0.80	24.5	1.14	34.8
SPECCA, MJ_{LHV}/kg_{CO2}	3.60		3.75	

In the CaL configuration shown in Fig. 2, the carbonator of the CaL process is placed between the outlet of the suspension preheater and the raw mill. However, for the ease of retrofit, it would be preferable to place the carbonator downstream the raw mill, which would avoid any change in the operation of the mill. The effect of such a plant configuration is that the gas treated in the carbonator becomes highly diluted with air, due to air in-leakage in the raw mill, causing a significant increase of the flue gas flow rate to be treated in the carbonator and a corresponding decrease of the CO_2 concentration.

Starting from the selected CaL base case with IL = 20%, Ws = 1000 kg/m^2 and E_{carb} = 90%, the effect of placing the carbonator of the CaL system after the raw mill is assessed. Results obtained for both cases are reported in Table 7. Considering a typical air leak of 38.8 kg/s in the mill, the flue gas flow rate to be treated in the carbonator increases by 70% and CO_2 concentration reduces from 27.6% to 19.2%. The higher flow rate results in a proportionally higher carbonator reactor cross-section to keep the design gas superficial velocity. The total solid inventory (in kg) in the carbonator is increased to keep the design specific inventory of 1000 kg per m^2 of cross section, leading to a larger inventory for a given flow rate of CO_2 entering the carbonator. However, because of the reduced kinetics caused by the reduced CO_2 partial pressure, solid circulation between calciner and carbonator reactors (F_{Ca}/F_{CO2}) slightly increases when the carbonator is placed after the raw mill, to maintain the same CO_2 capture efficiency in the carbonator of the base case.

When the carbonator is placed after the raw mill, the temperature of the gas at the carbonator inlet and convective pass outlet reduce compared to the reference case. Carbonator inlet temperature (i.e. raw mill outlet temperature) reduces from 328 °C of the base case to 110 °C and convective section outlet temperature (i.e. temperature of decarbonized flue gas at the stack) reduces from 430 °C of the base case to 120 °C. Therefore, the sensible heat associated to the gas heating within the carbonator is comparable with the base case, despite the much larger flow rate. As a consequence, changing the position of the carbonator in the cement plant does not have a significant impact neither on the total heat input nor on the SPECCA, as shown in Table 7.

Regarding this configuration, it has to be remarked that the carbonator will have to operate in a much wider range of gas flow rates compared to the base case configuration. As a matter of fact, after yearly maintenance periods, the raw mill operates with reduced air leakages, leading to a gas flow rate about 15% lower than in the operation under the typical air leakages considered before (CEMCAP, 2017). Given the carbonator cross-section area, this reduction in the flow rate turns out in a decrease of the superficial gas velocity at the carbonator inlet from 5 m/s to 4.2 m/s, which will keep the bed under fast fluidization regime, with a sufficient solid transport capacity. A larger variation of the gas flow rate occurs during the so called “direct operation” time (about 10% of the day), when the preheater off-gas bypasses the raw mill. Under these conditions, gas volume flow rate reduces by about 45% and intended dilution with air or recycled flue gas may be necessary to keep a proper gas velocity and heat balance in the carbonator.

Based on these figures, it can be concluded that placing the carbonator before or after the raw mill will not affect the plant performance significantly. Therefore, the selection of the best position of the carbonator should be more based on engineering considerations related to the ease of retrofitting (favoring a post-raw mill carbonator), the cost and footprint of the CaL unit (favoring the pre-raw mill configuration, thanks to the smaller gas flow rate to be treated) and the stability of the operating conditions (favoring the pre-raw mill configuration, thanks to the smaller gas flow rate variation along the day and the year).

4.2. Effect of the heat recovery steam cycle efficiency

In the previous analysis, steam cycle parameters and turbine efficiency have been defined based on the current industrial practice in the design of steam cycles of similar size. When moving to larger steam cycles, which would occur in case the CaL process is integrated in a larger cement kiln than the reference one considered in this work, improved steam parameters (i.e. higher live steam temperature and pressure) and higher steam turbine efficiency are justified from an economic point of view, resulting in higher steam cycle efficiency. It is out of the scope of this work to carry out an economic assessment of the optimal steam cycle parameters, but a sensitivity analysis on the efficiency of the HRSC (i.e. the ratio between the net power output and the overall thermal input) has been carried out to analyze its effect on the global performance of the CaL cement kiln. In the analysis performed, it is assumed that the efficiency can change from a minimum of 20%,

which is typical of an organic Rankine cycle (ORC) for small heat inputs, to the maximum value of 45%, which is representative of a large scale state-of-the-art steam cycle and that may represent a case study where the steam produced by heat recovery from the CaL process is used in a nearby large steam power plant.

Fig. 9 shows the effect of the efficiency of the HRSC on the SPECCA for the four electric production scenarios considered in this work, for the CaL base case with IL = 20%, Ws = 1000 kg/m^2 and E_{carb} = 90%. As reported, the HRSC efficiency influences noticeably the SPECCA. For the fossil fuels based reference scenarios, a wide range of SPECCA values is obtained. For the USC coal-based power plant without CCS scenario, the SPECCA reduces from 7.0 MJ_{LHV}/kg_{CO2} with the steam cycle efficiency of 20% to 2.1 MJ_{LHV}/kg_{CO2} for efficiency of 45%. With the most advantageous reference technology of the PC subcritical power plant, the SPECCA achieves the lowest values among the four reference scenarios considered, reaching 1.2 MJ_{LHV}/kg_{CO2} for the highest HRSC efficiency of 45%. In case of the power generation scenario based on renewable energy sources, the performance is less affected by the steam cycle efficiency, featuring SPECCA between 7.2 and 5.4 MJ_{LHV}/kg_{CO2}.

4.3. Effect of deeper thermal integration

For the tail-end CaL configuration shown in Fig. 2, the CaO-rich solid purge extracted from the calcined solids is cooled down and then fed to the raw mill, where the relatively coarse particles from the fluidized bed CaL purge are milled to particle size suitable for clinker production. From a thermal integration point of view, it would be more efficient to feed the solid purge to the cement kiln preheating tower at high temperature, without any intermediate cooling step. Considering the average larger particle size in the CaL fluidized bed reactors (100–300 μm) compared to the size needed in the rotary kiln (10–20 μm), such a process configuration would be possible for example by collecting the purge stream from fines in the CaL off-gases, separated by high efficiency cyclones.

Main performance results obtained for this configuration are included in the second column of Table 8, where the hot purge from the CaL calciner at 920 °C is assumed to be fed to the rotary kiln. Compared to the base case, this configuration can reduce the fuel consumption in the pre-calciner by 6.5%, thanks to the higher sensible heat of the CaL purge fed to the clinker burning line. A secondary beneficial effect is related to the lower amount of CO_2 to be captured by the CaL process thanks to the lower fuel consumption in the pre-calciner, which reflects into a slightly lower fuel consumption in the CaL calciner. On the whole, a total fuel saving of 2.5% and a 2.3% better SPECCA (for the USC power generation scenario) is obtained with this better thermal integration compared to the base CaL case.

Another option for improving the heat integration of the process is to preheat the limestone make-up fed to the CaL process with the CO_2-rich off-gases at 920 °C from the CaL calciner. The results of this heat integration option, where the CaL make-up is assumed to be preheated to 750 °C, are included in the third column of Table 8. Heat input in the calciner of the CaL system is reduced by 4.2% with respect to the base case configuration, leading to lower electric power export and about 2% lower SPECCA than the base CaL case.

5. Conclusions

In this work, the integration of a tail-end Calcium looping (CaL) process into a cement plant is assessed, where the CaL carbonator is used as an end-of-pipe unit to capture the CO_2 produced both in the rotary kiln and in the pre-calciner of a conventional cement kiln. The performance results provided by detailed process simulations of the whole cement plant, including the CaL process, the Heat Recovery Steam Cycle and all the auxiliary units, show that:

- The CaL tail-end process can reduce direct CO_2 emissions from cement kilns by more than 90%. However, this process requires intrinsically high fuel consumptions (between twice to three times larger than a reference cement kiln without CO_2 capture), due to the double calcination needed for the CO_2 originating from limestone decomposition, which is first calcined in the air-blown cement kiln calciner and then re-calcined in the CaL oxyfuel calciner after it is captured in the carbonator. Increasing the integration level of the CaL unit in the cement kiln (i.e. increasing the fraction of $CaCO_3$ fed to the CaL unit rather than to the clinker burning line) reduces the double calcination effect and results in lower overall fuel consumptions. For this reason, high integration levels may be preferable for a cement kiln operator perspective, although this may make retrofitting less straightforward (see the dedicated comment below) and may be limited by the portion of high purity limestone used in the cement plant for raw meal preparation.
- High temperature heat available in the CaL process can be recovered by a steam cycle, producing sufficient power to fulfil the internal consumptions of the cement plant and of the capture section (mainly for oxygen production and CO_2 compression and purification). In this way, a CaL kiln becomes a net exporter of low CO_2 electric power in cases with low integration level, leading to possible emission credits on a life-cycle basis. In high integration level cases, total fuel consumption and power generated by the steam cycle reduce and the cement plant remains a net importer of electric power, although even with integration level of 80% the power generated by the steam cycle is sufficient to compensate the electric consumption of the capture plant (i.e. mainly ASU and CPU). It has

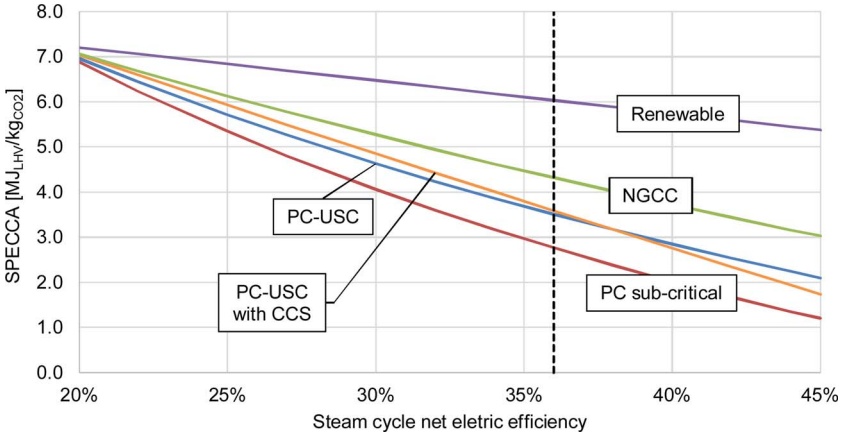

Fig. 9. SPECCA of the base CaL case with IL = 20%, Ws = 1000 kg/m^2 and E_{carb} = 90% as a function of the efficiency of the heat recovery steam cycle for the different power generation scenarios considered in this work.

Table 8
Main results of the CaL cement kiln configuration with tighter heat integration, compared to the CaL base case with IL = 20%, Ws = 1000 kg/m^2 and E_{carb} = 90%.

	Reference Ca-Looping case		Hot purge feed case		Make-up preheating case	
F_0/F_{CO2}	0.16		0.16		0.16	
F_{Ca}/F_{CO2}	4.78		4.78		4.79	
Total heat input (q), MW_{LHV} – MJ_{LHV}/kg_{clk}	284.3	8.67	279.8	8.45	276.0	8.42
Heat input in the rotary kiln, MW_{LHV} – MJ_{LHV}/kg_{clk}	39.7	1.21	39.7	1.20	39.7	1.21
Heat input in the pre-calciner, MW_{LHV} – MJ_{LHV}/kg_{clk}	50.6	1.54	47.7	1.44	50.6	1.54
Heat input in the Ca-Looping calciner, MW_{LHV} – MJ_{LHV}/kg_{clk}	194.1	5.92	192.4	5.81	185.8	5.67
Power balance						
Gross steam turbine electricity production, MW_e – kWh_e/t_{clk}	66.16	560.6	65.48	549.5	62.75	531.7
Steam cycle pumps and auxiliaries, MW_e – kWh_e/t_{clk}	−2.39	−20.24	−2.78	−23.35	−2.25	−19.07
Other auxiliaries, MW_e – kWh_e/t_{clk}	−49.50	−419.4	−49.60	−416.2	−48.82	−413.7
Net electricity production (P_e), MW_e – kWh_e/t_{clk}	14.27	120.9	13.10	109.9	11.68	99.0
Net electricity production (P_e), kWh_e/t_{cem}	89.1		81.0		73.0	
State of the art pulverized coal ultra-supercritical power plant						
Equivalent fuel consumption (q_{eq}), MW_{LHV} – MJ_{LHV}/kg_{clk}	252.0	7.69	250.2	7.6	249.5	7.6
Direct CO_2 emission (e_{CO2}), kg/s – kg_{CO2}/t_{clk}	3.9	117.7	3.8	115.7	3.8	117.4
Equivalent CO_2 emission ($e_{CO2,eq}$), kg/s – kg_{CO2}/t_{clk}	0.8	24.5	1.0	31.1	1.3	41.1
SPECCA, MJ_{LHV}/kg_{CO2}	3.60		3.49		3.59	

to be noted that the size of the steam cycle associated to the reference cement kiln producing 3000 tpd of clinker is one order of magnitude smaller than the steam cycle of a large-scale coal-fired power plant. Therefore, the heat recovery steam cycle will be based on a subcritical technology with efficiency of about 35%, which is noticeably lower than the efficiency of about 45% of a large ultra-supercritical steam cycle that is based on more advanced steam parameters and layout.

- Specific primary energy consumption for CO_2 avoided (SPECCA) index largely depends on the reference technology considered for power generation in the electric grid connected to the cement plant. This is because indirect fuel savings and CO_2 emission credits associated to power export/import depend on the specific technology that will balance the variation of the power exchanged with the grid. When considering the same fuel of the cement kiln (i.e. coal) as reference fuel for power generation, SPECCA values of 2.7-3.7 MJ/kg and 3.5-3.7 MJ/kg have been obtained when considering subcritical and ultra-supercritical reference technologies without CCS, respectively. These values are comparable with SPECCA of benchmark post-combustion and oxy-combustion technologies applied in power plants.

Since the SPECCA obtained is highly dependent on the efficiency of the heat recovery steam cycle and on the reference power generation technology, a wide sensitivity analysis on these two parameters has been performed. It has been demonstrated that SPECCA may range from a lower-bound limit of 1.2 MJ/kg, corresponding to a highly optimistic scenario where the cement plant features a 45% efficiency heat recovery steam cycle in an electricity market where electricity is generated with a 35% efficiency subcritical PC power plants, to an upper-bound value of 7.2 MJ/kg, obtained in a highly pessimistic scenario, where the cement plant features a poorly efficient 20% heat recovery steam or organic Rankine cycle in a power generation context based on zero CO_2 emissions renewable power plants.

- A retrofitting study has been performed, highlighting that the operation of the existing equipment of an existing cement kiln is not significantly affected by the integration of a CaL plant in case of low integration levels of the CaL unit. Gas velocity, gas-to-solids ratio and temperature profiles in the preheating tower barely change for integration levels below 25%. For the highest integration level assessed of 80%, gas flow rate and velocity in the preheater reduces by up to 17%, which may require modification of the risers inner diameter (e.g. by increasing the thickness of the refractory) or the addition of excess air for ensuring solids lifting in the preheating tower. On the other hand, the reduction of the gas flow rate in the preheating tower could also provide the opportunity of increasing the productivity of the cement kiln, increasing the gas flow rate by increasing the clinker production. The flexibility of the existing equipment (especially the clinker cooler) in accommodating a larger clinker production should be verified in this case.

The impact of the position of the CaL process with respect to the raw mill has been assessed. When placing the carbonator between the preheating tower and the raw mill a more compact carbonator (i.e. lower capital costs) and more stable gas flow rates to be treated (i.e. simpler operability) would result. On the other hand, placing the carbonator downstream the raw mill would facilitate the retrofittability of an existing plant because no change in the raw mill operation would be needed. From the energy efficiency and SPECCA point of view, minor effect of the position of the carbonator has been obtained.

- Alternative configurations based on a deeper thermal integration (i.e. hot CaL purge feed to the clinker burning line and CaL make-up solids preheating) have been assessed, showing the potential of rather small improvements in fuel consumption (−2.5 to 4.2%) and in the overall plant performance (~2% lower SPECCA) for the selected cases.

Acknowledgement

This project has received funding from the European Union's Horizon 2020 research and innovation Programme under grant agreement no 641185 (CEMCAP).

Appendix A

See Tables A1 and A2.

Table A1
Streams properties of base case CaL cement kiln with IL = 20%, Ws = 1000 kg/m^2 and E_{carb} = 90% shown in Fig. 2.

Stream		G	m[a]	T	%wt.												%vol.					
		[kg/s]	[kg/kg$_{clk}$]	[°C]	Al_2O_3	$CaCO_3$	CaO	Fe_2O_3	$H2O_{(L)}$	$MgCO_3$	MgO	SiO_2	C3S	C2S	C3A	$CaSO_4$	C4AF	Ar	CO_2	H_2O	O_2	N_2	SO_2
1	s	44.80	1.37	15.0	3.18	76.73	0.00	2.33	0.33	1.76	0.00	15.67	0.00	0.00	0.00	0.00	0.00						
2	s	5.94	0.18	920.0	6.48	0.00	81.10	0.80	0.00	0.00	0.34	8.72	0.00	0.00	0.00	2.55	0.00						
3	s	5.94	0.18	120.0	6.48	0.00	81.10	0.80	0.00	0.00	0.34	8.72	0.00	0.00	0.00	2.55	0.00						
4	g	73.18	2.23	15.0														0.92	0.03	1.03	20.73	77.28	0.00
5	g	17.80	0.54	15.0														3.00	0.00	0.00	95.00	2.00	0.00
6	g	17.80	0.54	150.0														3.00	0.00	0.00	95.00	2.00	0.00
7	s	7.19	0.22	60.0	69% C, 4% H, 0.5% S, 0.48% N, 9% O, 16.5% Ash, 0.5% Moisture, 0.02% Cl; LHV 27 MJ/kg																		
8	s	8.32	0.25	60.0	–	100	–	–	–	–	–	–	–	–	–	–	–						
9	g	39.97	1.22	315.4														2.19	40.26	6.04	50.00	1.51	0.00
10	g	70.19	2.14	920.1														1.39	80.52	12.07	5.00	1.03	0.00
11	g	70.19	2.14	400.0														1.39	80.52	12.07	5.00	1.03	0.00
12	g	22.17	0.68	400.0														1.39	80.52	12.07	5.00	1.03	0.00
13	g	22.17	0.68	427.0														1.39	80.52	12.07	5.00	1.03	0.00
14	g	48.02	1.46	400.0														1.39	80.52	12.07	5.00	1.03	0.00
15	g	48.02	1.46	320.0														1.39	80.52	12.07	5.00	1.03	0.00
16	g	48.02	1.46	278.3														1.39	80.52	12.07	5.00	1.03	0.00
17	g	48.02	1.46	80.0														1.39	80.52	12.07	5.00	1.03	0.00
18	g	61.72	1.88	328.6														0.73	27.61	4.77	5.22	61.67	0.00
	s	2.43	0.07	328.6	3.58	67.94	9.53	2.16	0.00	1.52	0.06	14.90	0.00	0.01	0.00	0.30	0.00						
19	g	61.72	1.88	328.5														0.73	27.61	4.77	5.22	61.67	0.00
	s	2.43	0.07	328.6	3.58	67.94	9.53	2.16	0.00	1.52	0.06	14.90	0.00	0.01	0.00	0.30	0.00						
20	g	41.07	1.25	650.0														0.97	4.10	6.32	6.92	81.70	0.00
21	g	41.07	1.25	430.5														0.97	4.10	6.32	6.92	81.70	0.00
22	s	203.30	6.20	650.0	5.82	23.10	59.93	0.72	0.00	0.00	0.30	7.84	0.00	0.00	0.00	2.29	0.00						
23	s	188.59	5.75	920.1	6.48	0.00	81.11	0.80	0.00	0.00	0.34	8.72	0.00	0.00	0.00	2.55	0.00						
24	s	182.66	5.57	920.1	6.48	0.00	81.10	0.80	0.00	0.00	0.34	8.72	0.00	0.00	0.00	2.55	0.00						
25	s	50.74	1.55	60.0	3.57	67.75	9.49	2.15	0.29	1.55	0.04	14.86	0.00	0.00	0.00	0.30	0.00						
26	g	60.78	1.85	508.0														0.74	28.13	4.41	5.02	61.71	0.00
	s	9.38	0.29	508.0	3.58	67.89	9.59	2.16	0.00	1.30	0.16	14.91	0.02	0.07	0.00	0.30	0.01						
27	s	57.54	1.76	328.6	3.58	67.94	9.53	2.16	0.00	1.52	0.06	14.90	0.00	0.01	0.00	0.30	0.00						
28	g	60.38	1.84	651.1														0.74	28.13	4.41	5.02	61.71	0.00
	s	9.50	0.29	651.1	3.62	67.56	9.98	2.18	0.00	0.00	0.80	14.93	0.13	0.44	0.03	0.31	0.02						
29	s	57.67	1.76	508.0	3.58	67.89	9.59	2.16	0.00	1.30	0.16	14.91	0.02	0.07	0.00	0.30	0.01						

(*continued on next page*)

Table A1 (*continued*)

Stream		G [kg/s]	m[a] [kg/kg$_{dk}$]	T [°C]	%wt. Al_2O_3	$CaCO_3$	CaO	Fe_2O_3	$H2O_{(L)}$	$MgCO_3$	MgO	SiO_2	C3S	C2S	C3A	$CaSO_4$	C4AF	%vol. Ar	CO_2	H_2O	O_2	N_2	SO_2
30	g	59.99	1.83	761.0														0.73	28.55	4.46	4.78	61.48	0.00
	s	10.07	0.31	761.0	3.82	56.83	16.77	2.28	0.00	0.00	0.85	14.90	0.89	2.97	0.19	0.35	0.15						
31	s	58.24	1.78	651.1	3.62	67.56	9.98	2.18	0.00	0.00	0.80	14.93	0.13	0.44	0.03	0.31	0.02						
32	g	59.59	1.82	860.2														0.73	28.76	4.48	4.66	61.36	0.00
	s	12.41	0.38	860.2	4.76	6.46	48.65	2.78	0.00	0.00	1.10	14.75	4.44	14.82	0.93	0.54	0.76						
33	s	60.57	1.85	761.0	3.82	56.83	16.77	2.28	0.00	0.00	0.85	14.90	0.89	2.97	0.19	0.35	0.15						
34	s	38.42	1.17	860.2	4.76	6.46	48.65	2.78	0.00	0.00	1.10	14.75	4.44	14.82	0.93	0.54	0.76						
35	g	0.57	0.02	15.0														0.92	0.03	1.03	20.73	77.28	0.00
36	g	3.29	0.10	15.0														0.92	0.03	1.03	20.73	77.28	0.00
37	s	1.87	0.06	60.0	69% C, 4% H, 0.5% S, 0.48% N, 9% O, 16.5% Ash, 0.5% Moisture, 0.02% Cl; LHV 27 MJ/kg																		
38	s	1.47	0.04	60.0	69% C, 4% H, 0.5% S, 0.48% N, 9% O, 16.5% Ash, 0.5% Moisture, 0.02% Cl; LHV 27 MJ/kg																		
39	g	26.19	0.80	1137														0.92	0.03	1.03	20.73	77.28	0.00
	s	0.69	0.02	1137	0.00	0.00	0.77	0.00	0.00	0.00	1.14	0.00	64.39	14.02	9.55	0.63	9.50						
40	g	78.47	2.39	15.0														0.92	0.03	1.03	20.73	77.28	0.00
41	g	41.31	1.26	284.9														0.92	0.03	1.03	20.73	77.28	0.00
	s	1.19	0.04	284.9	0.00	0.00	0.77	0.00	0.00	0.00	1.14	0.00	64.39	14.02	9.55	0.63	9.50						
42	g	10.97	0.33	1137														0.92	0.03	1.03	20.73	77.28	0.00
	s	0.27	0.01	1137	0.00	0.00	0.77	0.00	0.00	0.00	1.14	0.00	64.39	14.02	9.55	0.63	9.50						
43[a]	g	2.84	0.09	23.5														11.49	36.92	0.00	40.08	11.50	0.00
44	g	42.57	1.30	36.0														0.79	95.88	0.00	2.97	0.35	0.00
45	s	32.79	1.00	114.9	0.00	0.00	0.77	0.00	0.00	0.00	1.14	0.00	64.39	14.02	9.55	0.63	9.50						

[a] CPU vent gas to atmosphere.

Table A2
Streams properties of the heat recovery steam cycle of the base case CaL cement kiln with IL = 20%, Ws = 1000 kg/m^2 and E_{carb} = 90% shown in Fig. 3.

Stream	G [kg/s]	T [°C]	P [bar]
SC-1	61.88	532	105.26
SC-2	61.88	530	100.00
SC-3	52.21	39	0.070
SC-4	55.35	39	0.070
SC-5	55.35	39	5.62
SC-6	55.35	70	4.62
SC-7	55.35	83	3.62
SC-8	61.88	140	3.62
SC-9	61.88	142	134.42
SC-10	61.88	156	130.34
SC-11	61.88	173	125.44
SC-12	61.88	209	114.42
SC-13	61.88	321	114.42
SC-14	3.15	73	0.36
SC-15	3.15	44	0.34
SC-16	3.15	39	0.07
SC-17	6.07	165	3.89
SC-18	0.46	165	3.89
SC-19	0.46	140	3.62
SC-20	1.00	165	3.89
SC-21	1.00	140	3.62

References

Abanades, J.C., Arias, B., Lyngfelt, A., Mattisson, T., Wiley, D.E., Li, H., Ho, M.T., Mangano, E., Brandani, S., 2015. Emerging CO_2 capture systems. Int. J. Greenh. Gas Control 40, 126–166. http://dx.doi.org/10.1016/j.ijggc.2015.04.018.

Abanades, J.C., 2002. The maximum capture efficiency of CO_2 using a carbonation/calcination cycle of CaO/$CaCO_3$. Chem. Eng. J. 90, 303–306. http://dx.doi.org/10.1016/S1385-8947(02)00126-2.

Arias, B., Diego, M.E., Abanades, J.C., Lorenzo, M., Diaz, L., Martínez, D., Alvarez, J., Sánchez-Biezma, A., 2013. Demonstration of steady state CO_2 capture in a 1.7MW_{th} calcium looping pilot. Int. J. Greenh. Gas Control 18, 237–245. http://dx.doi.org/10.1016/j.ijggc.2013.07.014.

Arias, B., Alonso, M., Abanades, C., 2017. CO_2 capture by calcium looping at relevant conditions for cement plants: experimental testing in a 30 kW_{th} pilot plant. Ind. Eng. Chem. Res. 56, 2634–2640. http://dx.doi.org/10.1021/acs.iecr.6b04617.

Atsonios, K., Grammelis, P., Antiohos, S.K., Nikolopoulos, N., Kakaras, E., 2015. Integration of calcium looping technology in existing cement plant for CO2 capture: process modeling and technical considerations. Fuel 153, 210–223. http://dx.doi.org/10.1016/j.fuel.2015.02.084.

Barin, I., 1995. Thermochemical Data of Pure Substances, third ed. VCH.

Bosoaga, A., Masek, O., Oakey, J.E., 2009. CO_2 capture technologies for cement industry. Energy Procedia 133–140. http://dx.doi.org/10.1016/j.egypro.2009.01.020.

CEMCAP, 2016. D4.1: Design and Performance of CEMCAP Cement Plant Without CO_2 Capture. www.sintef.no/projectweb/cemcap/results/.

CEMCAP, 2017. D3.2: CEMCAP Framework for Comparative Techno-economic Analysis of CO2 Capture from Cement Plants. www.sintef.no/projectweb/cemcap/results/.

Charitos, A., Rodríguez, N., Hawthorne, C., Alonso, M., Zieba, M., Arias, B., Kopanakis, G., Scheffknecht, G., Abanades, J.C., 2011. Experimental validation of the calcium looping CO_2 capture process with two circulating fluidized bed carbonator reactors. Ind. Eng. Chem. Res. 50, 9685–9695. http://dx.doi.org/10.1021/ie200579f.

Consonni, S., Viganò, F., 2012. Waste gasification vs. conventional waste-to-energy: a comparative evaluation of two commercial technologies. Waste Manag. 32, 653–666. http://dx.doi.org/10.1016/j.wasman.2011.12.019.

Dean, C.C., Blamey, J., Florin, N.H., Al-Jeboori, M.J., Fennell, P.S., 2011a. The calcium looping cycle for CO_2 capture from power generation, cement manufacture and hydrogen production. Chem. Eng. Res. Des. 89, 836–855. http://dx.doi.org/10.1016/j.cherd.2010.10.013.

Dean, C.C., Dugwell, D., Fennell, P.S., 2011b. Investigation into potential synergy between power generation, cement manufacture and CO_2 abatement using the calcium looping cycle. Energy Environ. Sci. 4, 2050. http://dx.doi.org/10.1039/c1ee01282g.

EBTF, 2011. European Best Practice Guidelines for Assessment of CO_2 Capture Technologies. EBTF.

Estabrook, J.E., Leger, R.H., 2002. Steam turbines for industrial applications. GE Power Syst. 1, 1–30.

European Union, 2004. L32/183: establishing harmonised efficiency reference values for separate production of electricity and heat in application of Directive 2004/8/EC of the European Parliament and of the Council. Off. J. Eur. Union.

Gardiner, W.C., 1984. Combustion Chemistry. Springer-Verlag, New York.

Gecos, 2013. GS software [WWW Document].

Grasa, G.S., Abanades, J.C., 2006. CO_2 capture capacity of CaO in long series of carbonation/calcination cycles. Ind. Eng. Chem. Res. 45, 8846–8851. http://dx.doi.org/10.1021/ie0606946.

Grasa, G.S., Abanades, J.C., Alonso, M., González, B., 2008. Reactivity of highly cycled particles of CaO in a carbonation/calcination loop. Chem. Eng. J. 137, 561–567. http://dx.doi.org/10.1016/j.cej.2007.05.017.

Hills, T., Leeson, D., Florin, N., Fennell, P., 2016. Carbon capture in the cement industry: technologies, progress, and retrofitting. Environ. Sci. Technol. 50, 368–377. http://dx.doi.org/10.1021/acs.est.5b03508.

Hoenig, V., Hoppe, H., Koring, K., Lemke, J., 2012. ECRA CCS Project – Report on Phase III. TR-ECRA-119/2012.

Hornberger, M., Spörl, R., Scheffknecht, G., 2017. Calcium looping for CO_2 capture in cement plants – pilot scale test. Energy Procedia 114, 6171–6174. http://dx.doi.org/10.1016/j.egypro.2017.03.1754.

IEA, 2009. Cement Technology Roadmap 2009: Carbon Emissions Reductions up to 2050. IEAhttp://dx.doi.org/10.1787/9789264088061.

IEA, 2015. CO_2 Emissions from Fuel Combustion 2015 Edition. IEA Statisticshttp://dx.doi.org/10.1787/co2_fuel-2015-en.

IEAGHG, 2005. Oxy Combustion Processes for CO_2 Capture from Power Plant. Report number 2005/9.

IEAGHG, 2008. CO_2 Capture in the Cement Industry. Technical Study. Report Number 2008/3.

IEAGHG, 2013. Deployment of CCS in the Cement Industry. Report 2013/19.

IEAGHG, 2014. Evaluation and Analysis of the Performance of Dehydration Units for CO_2 Capture. Report number 2014/04.

Kunii, D., Levenspiel, O., 1997. Circulating fluidized-bed reactors. Chem. Eng. Sci. 52, 2471–2482. http://dx.doi.org/10.1016/S0009-2509(97)00066-3.

Kvamsdal, H.M., Romano, M.C., van der Ham, L., Bonalumi, D., van Os, P., Goetheer, E., 2014. Energetic evaluation of a power plant integrated with apiperazine-based CO_2 capture process. Int. J. Greenh. Gas Control 28, 343–355. http://dx.doi.org/10.1016/j.ijggc.2014.07.004.

Marchi, M.I., Cinti, G., Romano, M.C., Campanari, S., Consonni, S., 2012a. Improved process for the production of cement clinker and related apparatus (in Italian). Patent MI2012 A00382.

Marchi, M.I., Cinti, G., Romano, M.C., Campanari, S., Consonni, S., 2012b. Process and improved plant for the production of cement clinker (in Italian). Patent MI2012 A00383.

Martínez Vera E.R., 2009. Method for capturing CO_2 produced by cement plants by using the calcium cycle. US 2009/0255444 A1.

Martínez, I., Grasa, G., Murillo, R., Arias, B., Abanades, J.C., 2013. Modelling the continuous calcination of $CaCO_3$ in a Ca-looping system. Chem. Eng. J. 215–216. http://dx.doi.org/10.1016/j.cej.2012.09.134.

Martínez, I., Grasa, G., Parkkinen, J., Tynjälä, T., Hyppänen, T., Murillo, R., Romano, M.C., 2016. Review and research needs of Ca-Looping systems modelling for post-combustion CO_2 capture applications. Int. J. Greenh. Gas Control 50, 271–304. http://dx.doi.org/10.1016/j.ijggc.2016.04.002.

Matschei, T., Lothenbach, B., Glasser, F.P., 2007. Thermodynamic properties of Portland cement hydrates in the system $CaO-Al_2O_3-SiO_2-CaSO_4-CaCO_3-H_2O$. Cem. Concr. Res. 37, 1379–1410. http://dx.doi.org/10.1016/j.cemconres.2007.06.002.

Olivier, J.G.J., Janssens-Maenhout, G., Muntean, M., Peters, J.A.H.W., 2016. Trends in Global CO_2 Emissions: 2016 Report. PBL Netherlands Environmental Assessment Agency; Ispra: European Commission, Joint Research Centre, The Hague.

Ozcan, D.C., Ahn, H., Brandani, S., 2013. Process integration of a Ca-looping carbon capture process in a cement plant. Int. J. Greenh. Gas Control 19, 530–540. http://dx.doi.org/10.1016/j.ijggc.2013.10.009.

Pipitone, G., Bolland, O., 2009. Power generation with CO_2 capture: technology for CO_2 purification. Int. J. Greenh. Gas Control 3, 528–534. http://dx.doi.org/10.1016/j.ijggc.2009.03.001.

Queneau, P.E., Marcuson, S.W., 1996. Oxygen pyrometallurgy at copper cliff-A half century of progress. JOM 48, 14–21. http://dx.doi.org/10.1007/BF03221355.

Rodríguez, N., Murillo, R., Abanades, J.C., 2012. CO_2 capture from cement plants using oxyfired precalcination and/or calcium looping. Environ. Sci. Technol. 46,

2460–2466. http://dx.doi.org/10.1021/es2030593.
Romano, M.C., Spinelli, M., Campanari, S., Consonni, S., Marchi, M., Pimpinelli, N., Cinti, G., 2014. The calcium looping process for low CO_2 emission cement plants. Energy Procedia 61, 500–503. http://dx.doi.org/10.1016/j.egypro.2014.11.1158.
Romano, M.C., 2012. Modeling the carbonator of a Ca-looping process for CO_2 capture from power plant flue gas. Chem. Eng. Sci. 69, 257–269. http://dx.doi.org/10.1016/j.ces.2011.10.041.
Romano, M.C., 2013. Ultra-high CO_2 capture efficiency in CFB oxyfuel power plants by calcium looping process for CO_2 recovery from purification units vent gas. Int. J. Greenh. Gas Control 18, 57–67. http://dx.doi.org/10.1016/j.ijggc.2013.07.002.
Scholes, C.A., Ho, M.T., Aguiar, A.A., Wiley, D.E., Stevens, G.W., Kentish, S.E., 2014. Membrane gas separation processes for CO_2 capture from cement kiln flue gas. Int. J. Greenh. Gas Control 24, 78–86. http://dx.doi.org/10.1016/j.ijggc.2014.02.020.
Schorcht, F., Kourti, I., Scalet, B., Roudier, S., Delgado Sancho, L., 2013. JRC Reference Reports- Best Available Techniques (BAT) Reference Document for the Production of Cement, Lime and Magnesium Oxide. 10.2788/12850.
Shah, M.M., 2011. Carbon dioxide (CO_2) compression and purification technology for oxy-fuel combustion. Capture. http://dx.doi.org/10.1016/B978-1-84569-671-9.50011-9.
Shimizu, T., Hirama, T., Hosoda, H., Kitano, K., Inagaki, M., Tejima, K., 1999. A twin fluid-bed reactor for removal of CO_2 from combustion processes. Chem. Eng. Res. Des. 77, 62–68. http://dx.doi.org/10.1205/026387699525882.
Siemens 2009, 2009. Industrial Steam Turbines – the comprehensive product range from 2 to 250 megawatts. Ind. Steam Turbines 1, 1–8.
Spinelli, M., Martínez, I., De Lena, E., Cinti, G., Hornberger, M., Spörl, R., Abanades, J.C., Becker, S., Mathai, R., Fleiger, K., Hoenig, V., Gatti, M., Scaccabarozzi, R., Campanari, S., Consonni, S., Romano, M.C., 2017. Integration of Ca-Looping systems for CO_2 capture in cement plants. Energy Procedia 114, 6206–6214. http://dx.doi.org/10.1016/j.egypro.2017.03.1758.
Spliethoff, H., 2010. Power Generation from Solid Fuels, Power Systems. Springer-Verlag, Berlin, Heidelberg. http://dx.doi.org/10.1007/978-3-642-02856-4.
Ströhle, J., Junk, M., Kremer, J., Galloy, A., Epple, B., 2014. Carbonate looping experiments in a 1 MW_{th} pilot plant and model validation. Fuel 127, 13–22. http://dx.doi.org/10.1016/j.fuel.2013.12.043.
Stull, D.R., Prophet, H., 1971. JANAF Thermochemical Tables, 2nd ed. National Bureau of Standards, Washington D.C., USA.
Suhr, M., Klein, G., Kourti, I., Rodrigo Gonzalo, M., Giner Santonja, G., Roudier, S., Delgado Sancho, L., 2015. Best Available Techniques (BAT). Reference Document for the Production of Cement, Lime and Magnesium Oxide. 10.2788/12850.
Telesca, A., Calabrese, D., Marroccoli, M., Tomasulo, M., Valenti, G.L., Duelli, G., Montagnaro, F., 2014. Spent limestone sorbent from calcium looping cycle as a raw material for the cement industry. Fuel 118, 202–205. http://dx.doi.org/10.1016/j.fuel.2013.10.060.
Telesca, A., Marroccoli, M., Tomasulo, M., Valenti, G.L., Dieter, H., Montagnaro, F., 2015. Calcium looping spent sorbent as a limestone replacement in the manufacture of Portland and calcium sulfoaluminate cements. Environ. Sci. Technol. 49, 6865–6871. http://dx.doi.org/10.1021/acs.est.5b00394.
Trevino, V.L., Martínez, E.R., 2009. Method for capturing CO_2 produced by cement plant by using the calcium cycle. EP 2461892A1.
Vatopoulos, K., Tzimas, E., 2012. Assessment of CO_2 capture technologies in cement manufacturing process. J. Clean. Prod. 32, 251–261. http://dx.doi.org/10.1016/j.jclepro.2012.03.013.